

Adaptive Training for Correlated Fading Channels with Feedback

Manish Agarwal, Michael Honig, and Baris Ata

Northwestern University

{m-agarwal,mh,b-ata}@northwestern.edu

June 7, 2018

Abstract

We consider data transmission through a time-selective, correlated (first-order Markov) Rayleigh fading channel subject to an average power constraint. The channel is estimated at the receiver with a pilot signal, and the estimate is fed back to the transmitter. The estimate is used for coherent demodulation, and to adapt the data and pilot powers. We explicitly determine the optimal pilot and data power control policies in a continuous-time limit where the channel state evolves as an Ornstein-Uhlenbeck diffusion process, and is estimated by a Kalman filter at the receiver. The optimal pilot policy switches between zero and the maximum (peak-constrained) value (“bang-bang” control), and approximates the optimal discrete-time policy at low Signal-to-Noise Ratios (equivalently, large bandwidths). The switching boundary is defined in terms of the system state (estimated channel mean and associated error variance), and can be explicitly computed. Under the optimal policy, the transmitter conserves power by decreasing the training power when the channel is faded, thereby increasing the data rate. Numerical results show a significant increase in achievable rate due to the adaptive training scheme with feedback, relative to constant (non-adaptive) training, which does not require feedback. The gain is more pronounced at relatively low SNRs and with fast fading. Results are further verified through Monte Carlo simulations.

Index Terms

Limited-rate feedback, Gauss-Markov channel, channel estimation, adaptive training, wideband channel, diffusion approximation, free boundary problems, Bang-Bang control, Variational Inequalities.

This work was supported by the U.S. Army Research Office under grant W911NF-07-1-0028 and NSF under grant CCR-0310809. This paper was presented in part at the IEEE International Symposium on Information Theory (ISIT), Seattle, USA, July, 2006 and at the Information Theory and its Applications (ITA), San Diego, January, 2008.

I. INTRODUCTION

The achievable rate for a time-selective fading channel depends on what channel state information (CSI) is available at the receiver and transmitter. Namely, CSI at the receiver can increase the rate by allowing coherent detection, and CSI at the transmitter allows adaptive rate and power control (e.g., see [1, Ch. 6]). Obtaining CSI at the receiver and/or transmitter requires overhead in the form of a pilot signal and feedback.

We consider a correlated time-selective flat Rayleigh fading channel, which is unknown at both the receiver and transmitter. The transmitter divides its power between a pilot, used to estimate the channel at the receiver, and the data. Given an average transmitted power constraint, our problem is to optimize the instantaneous pilot and data powers as functions of the time-varying channel realization. Our performance objective is a lower bound on the achievable rate, which accounts for the channel estimation error.

Power control with channel state feedback, assuming the channel is perfectly known at the receiver, has been considered in [2]–[6]. There the focus is on optimizing the input distribution for different channel models using criteria such as rate maximization and outage minimization. Optimal power allocation in the presence of channel estimation error has been considered in [7], [8]. The problem of optimal pilot design for a variety of fading channel models has been considered in [9]–[15]. There the pilot power and placement, once optimized, is fixed and is not adapted with the channel conditions. A key difference here is that the transmitter uses the CSI to adapt *jointly* the instantaneous data and pilot powers. Because the channel is correlated in time, adapting the pilot power with the estimated channel state can increase the achievable rate. We also remark that although we analyze a single narrowband fading channel, our results apply to a set of parallel fading Gaussian channels, where the average power is split over all channels.

We start with a correlated block fading model in which the sequence of channel gains is Gauss-Markov¹ with known statistics at the receiver. The channel estimate is updated at the beginning of each block using a Kalman filter, and determines the power for the data, and the power for the pilot symbols in the succeeding coherence block. Optimal power control policies are specified implicitly through a Bellman equation [20]. Other dynamic programming formulations of power

¹Several theoretical and measurement based studies, such as [16]–[19], have argued that this is a reasonable model for time-selective wireless channels.

control problems have been presented in [6], [21]–[24], although in that work the channel is either known perfectly (perhaps with a delay), or is unknown and not estimated.

Because an analytical solution to the Bellman equation appears to be difficult to obtain, we study a diffusion limit in which the correlation between successive coherence blocks tends to one and the average power goes to zero. (This corresponds to a wideband channel model in which the available power is divided uniformly over a large number of parallel flat Rayleigh fading sub-channels.) In this limit, the Gauss-Markov channel becomes a continuous-time Ornstein-Uhlenbeck process [25], and the Bellman equation becomes a partial differential equation (PDE). A diffusion equation is also derived, which describes the evolution of the state (channel estimate and the associated error variance), given a power allocation policy. In this limit, we show that given a peak power constraint for the pilot power, the optimal pilot power control policy is a switching policy (“bang-bang” control): the pilot power is either the maximum allowable or zero, depending upon the current state. Hence the optimal pilot power control policy requires at most one feedback bit per coherence block. Also, the optimal data power control policy is found to be a variation of waterfilling [1]. Other work in which the wireless channel is modeled as a diffusion process is presented in [23], [26].

The switching points for the optimal policy form a contour in the state space, which is referred to as the *free boundary* for the corresponding PDE. Solving this PDE then falls in the class of *free boundary problems* [27], [28]. We show that in the diffusion limit the system state becomes confined to a narrow region along the boundary. Furthermore, the associated probability distribution over the boundary is exponential. That enables a numerical characterization of the boundary shape.

Our results show that the average pilot power should decrease as the channel becomes more severely faded. We observe that the optimal switching policy is equivalent to adapting the pilot symbol insertion rate with *fixed* pilot symbol energy.² The optimal pilot insertion rate as a function of the channel estimate is then determined by the shape of the free boundary. We show that the boundary shape essentially shifts pilot power from more probable (faded) states to less probable (good) states. Furthermore, the boundary shape guarantees that the channel estimate is

²Alternatively, the same performance can be achieved by fixing the pilot insertion rate and varying the pilot power. However, in principle that would require infinite-precision feedback in contrast to bang-bang control, which requires one feedback bit per coherence block.

sufficiently accurate to guide the power adaptation.

Numerical results show that pilot power adaptation can provide substantial gains in achievable rates (up to a factor of two). The gains are more pronounced at low SNRs and with fast fading channels. Although these results are derived in the limit of large bandwidth (low SNR), Monte Carlo simulations show that they provide an accurate estimate of the performance when the bandwidth is large but finite (a few hundred coherence bands). Moreover, the optimal switching policy in the diffusion limit accurately approximates the optimal pilot power control policy for the discrete-time model, and provides essentially the same performance gains relative to constant pilot power.

To limit the overall feedback rate, we also consider combining the adaptive pilot power with “on-off” data power control, which also switches between a fixed positive value and zero. (Hence that also requires at most one bit feedback per coherence block.) The corresponding optimal free boundaries are computed, and results show that this scheme gives negligible loss in the achievable rate.

The next section presents the system model and Section III formulates the pilot optimization problem as a dynamic program. Section IV presents the associated diffusion limit and the corresponding Bellman equation. The optimal policy is then characterized in Sections V-VII with optimal data power control, and in Section VIII with optimal on-off data power control. Numerical results showing free boundaries and the corresponding performance are also presented in Sections VII and VIII. Training overhead is discussed in Section IX, and conclusions and remaining issues are discussed in Section X.

II. CORRELATED BLOCK FADING MODEL

We start with a block fading channel model in which each coherence block contains M symbols, consisting of T pilot symbols and D data symbols. The vector of channel outputs for coherence block i is given by

$$\mathbf{y}_i = h_i \begin{pmatrix} \sqrt{P_{i;T}} \mathbf{S}_{i;T} \\ \sqrt{P_i} \mathbf{S}_i \end{pmatrix} + \mathbf{z}_i \quad (1)$$

where $\mathbf{S}_{i;T}$ and \mathbf{S}_i are, respectively, vectors containing the pilot and data symbols, each with unit variance, and $P_{i;T}$ and P_i are the associated pilot and data powers. The noise \mathbf{z}_i contains circularly symmetric complex Gaussian (CSCG) random variables, and is white with covariance

$\sigma_z^2 \mathbf{I}$. The channel gain h_i is also CSCG, is constant within the block, and evolves from block to block according to a Gauss-Markov process, i.e.,

$$h_{i+1} = r h_i + \sqrt{1 - r^2} w_i \quad (2)$$

where w_i is an independent CSCG random variable with mean zero and variance σ_h^2 , and $r \in [0, 1]$ determines the correlation between successive blocks. We will assume that r and σ_h^2 are known at the receiver. The training energy per symbol in block i is defined as $\epsilon_i = \alpha P_{i;T}$, where $\alpha = T/M$. In what follows, it will be convenient to write $P_{i;T}$ as ϵ_i/α .

The receiver updates the channel estimate during each coherence block with a Kalman filter [29], given the model (2) and the pilot symbols, and relays the estimate back to the transmitter. The feedback occurs between the pilot and data symbols, and is assumed to occupy an insignificant fraction of the coherence time. We re-write the noise vector \mathbf{z}_i as $[\mathbf{z}_{i;T}^\dagger \mathbf{z}_i^\dagger]^\dagger$ where $\mathbf{z}_{i;T}$ and \mathbf{z}_i are, respectively, $T \times 1$ and $D \times 1$ vectors and $[\cdot]^\dagger$ denotes Hermitian transpose. The channel estimate \hat{h}_i and estimation error $\theta_i = E(|h_i|^2) - E(|\hat{h}_i|^2)$ evolve according to the following Kalman filter updates:

$$\hat{h}_{i+1} = r \hat{h}_i + g_{i+1} \sqrt{\frac{\epsilon_{i+1}}{\alpha}} T e_{i+1|i} + g_{i+1} \mathbf{S}_{i+1;T}^\dagger \mathbf{z}_{i+1;T} \quad (3)$$

$$\theta_{i+1} = \frac{\sigma_z^2 \theta_{i+1|i}}{\epsilon_i M \theta_{i+1|i} + \sigma_z^2} \quad (4)$$

where

$$g_i = \sqrt{\frac{\epsilon_i}{\alpha}} \frac{\theta_i}{\sigma_z^2} \quad (5)$$

$$e_{i+1|i} = h_{i+1} - r \hat{h}_i \quad (6)$$

$$\theta_{i+1|i} = r^2 \theta_i + (1 - r^2) \sigma_h^2. \quad (7)$$

It is straightforward to show that the channel estimate \hat{h}_i in (3) does not depend on T . (What is important is the total pilot energy per coherence block.) Hence the data rate is maximized by taking $T = 1$ with fixed ϵ_i (i.e., the training power $P_{i;T} = \epsilon_i M$). Training therefore requires an overhead of $1/M$ fraction of the channel uses. We ignore this overhead for the time being and focus on optimizing the training power ϵ_i . This issue is revisited in Sec. IX.

We wish to determine P_i and ϵ_i , which maximize the achievable rate. Specifically, the channel estimate \hat{h}_i and variance θ_i determine the data power in the *current* coherence block, P_i , and the

pilot power in the *next* coherence block, ϵ_{i+1} . We assume that the transmitter codes over many coherence blocks, and use the following lower bound on ergodic capacity, which accounts for channel estimation error, as the performance objective [11], [30],

$$R(P_i, \hat{\mu}_i, \theta_i) = \log \left(1 + \frac{P_i \hat{\mu}_i}{P_i \theta_i + \sigma_z^2} \right) \quad (8)$$

where $\hat{\mu}_i = |\hat{h}_i|^2$. In the next section, we formulate the joint pilot and data power optimization problem, and subsequently characterize the optimal power control policy implicitly as the solution to a discrete-time Bellman equation.

III. DYNAMIC PROGRAMMING FORMULATION

The pilot and data power control problem can be stated as

$$\begin{aligned} & \max_{\{P_i, \epsilon_i\}} \liminf_{n \rightarrow \infty} \frac{1}{n} E \left[\sum_{i=0}^{n-1} R(P_i, \hat{\mu}_i, \theta_i) \right] \\ & \text{subject to: } \limsup_{n \rightarrow \infty} E \left[\frac{1}{n} \sum_{i=0}^{n-1} \epsilon_i + \frac{1}{n} \sum_{i=0}^{n-1} P_i \right] \leq P_{av}, \end{aligned} \quad (9)$$

$$\text{and } \epsilon_i \leq \epsilon_{max},$$

where the expectation is over the sequence of channel gains. We have imposed an additional peak power constraint on the training power. This is a discrete-time Markov control problem, so that the solution can be formulated as an infinite-horizon dynamic program with an average value objective. The system state at time (block) i is $S_i = (\hat{\mu}_i, \theta_i)$, and the action maps the state to the power pair (P_i, ϵ_{i+1}) . To see that S_i is the system state, note that $e_{i+1|i}$ in (6) and \hat{h}_i are independent random variables, hence it follows from (3) and (4) that the probability distribution of S_{i+1} is determined only by S_i and the action ϵ_{i+1} . The process $\{(\hat{\mu}_i, \theta_i)\}$ is therefore a Markov chain driven by the control $\{\epsilon_i\}$.

The average power constraint in (9) can be included in the objective through a Lagrange multiplier giving the relaxed problem

$$\max_{P_i, 0 \leq \epsilon_i \leq \epsilon_{max}} \liminf_{n \rightarrow \infty} \frac{1}{n} E \left[\sum_{i=0}^{n-1} [R(P_i, \hat{\mu}_i, \theta_i) - \lambda (\epsilon_i + P_i)] \right] \quad (10)$$

where λ is chosen to enforce the constraint (9). If there exists a bounded function $V(\hat{\mu}, \theta)$ and a constant C , which satisfy the Bellman equation

$$V(\hat{\mu}, \theta) + C = \max_{P, 0 \leq \epsilon \leq \epsilon_{max}} [R(P, \hat{\mu}, \theta) - \lambda (\epsilon + P) + E_{\epsilon, (\hat{\mu}, \theta)}[V]] , \quad (11)$$

then an optimal policy maximizes the right-hand side [20]. The function $V(\cdot, \cdot)$ is called an “auxiliary value function”, and C is the maximum value of the objective in (10). The expectation $E_{\epsilon, (\hat{\mu}, \theta)}[\cdot]$ is over the conditional probability of S_{i+1} given $S_i = (\hat{\mu}, \theta)$ and action $\epsilon_{i+1} = \epsilon$.

Using the channel state evolution equations derived in Section II, we have

$$E_{\epsilon, (\hat{\mu}, \theta)}[V] = \int_0^\infty V(u, \theta_{i+1}) f_{\hat{\mu}_{i+1}|S_i}(u) du \quad (12)$$

where $f_{\hat{\mu}_{i+1}|S_i}(u)$ is the conditional density of $\hat{\mu}_{i+1} = |\hat{h}_{i+1}|^2$ given $S_i = (\hat{\mu}_i, \theta_i) = (\hat{\mu}, \theta)$, and θ_{i+1} is given by (4). From (3) it follows that $f_{\hat{\mu}_{i+1}|S_i}(u)$ is Ricean with noncentrality parameter $r^2 \hat{\mu}$ and variance $[(\theta_{i+1|i} \epsilon M) / \sigma_z^2] \theta_{i+1} + r^2 \hat{\mu}$, where θ_{i+1} and $\theta_{i+1|i}$ are given by (4) and (7), respectively.

IV. DIFFUSION LIMIT

The Bellman equation (11) is an integral fixed point equation, and appears to be difficult to solve analytically. To gain insight into properties of optimal policies, we consider the following scaling, corresponding to a low SNR regime:

- 1) Time is scaled by the factor $1/N$, where $N \gg M$ is large, so that each coherence block of M symbols corresponds to $\delta t = \frac{M}{N}$ time units. Therefore one time unit in the scaled system contains $\frac{1}{\delta t} = \frac{N}{M}$ coherence blocks, or equivalently N channel uses.
- 2) The correlation between adjacent coherence blocks is $r = 1 - \rho(\delta t)$, where ρ is a constant. Hence this correlation goes to one as $N \rightarrow \infty$ (equivalently, the channel coherence time goes to zero), but with fixed correlation between blocks separated by N channel uses.
- 3) To maintain constant energy over N channel uses, the average power P_{av} , data power P_i , training power ϵ_i and the maximum training power ϵ_{max} are each scaled by $1/N$.

In the limit as $N \rightarrow \infty$, it can be shown that the discrete-time, complex, Gauss-Markov process $\{h_i\}$, given by (2), converges weakly to a continuous-time Ornstein-Uhlenbeck diffusion process $h(t)$ (e.g., see [31, Ch. 8]). Furthermore, the limiting channel process satisfies the stochastic differential equation (SDE)

$$dh(t) = -\rho h(t) dt + \sqrt{2\rho\sigma_h} dB(t), \quad (13)$$

where $B(t)$ is complex Brownian motion, and we assume that the initial state $h(0)$ is a CSCG random variable with zero mean and variance σ_h^2 . This is a Gauss-Markov process, which is

continuous in probability, and has autocorrelation function

$$\Phi(\tau) = \sigma_h^2 e^{-\rho\tau}, \quad (14)$$

where τ is the lag between the time samples of the channel. Hence ρ determines how fast the channel varies relative to the symbol rate. For example, the end-to-end normalized correlation across an interval of $\tau = 1$ (or, equivalently N channel uses) is $e^{-\rho}$.

The diffusion limit considered can be interpreted as *zooming out* on the channel and associated data transmission. Segments of the discrete channel process then become “compressed” in time, but with increasing correlation between successive coherence blocks so that the channel autocorrelation remains fixed. Prior work, which advocates the use of diffusion models for wireless channels is presented in [23], [26]. In this limit the Kalman filter continuously estimates the channel process, and the pilot and data powers are continuously updated based on continuous feedback. (We will see that to achieve optimal performance the feedback need not be continuous.) The optimal power control policy in the diffusion limit can then be interpreted as an approximation for the optimal discrete-time policy. (This will be illustrated numerically.)

The power scaling by $1/N$ can be interpreted as introducing N parallel, independent and statistically identical *sub-channels* over which the power is equally split. Hence the low SNR regime corresponds to a *wideband* channel.³

In the diffusion limit the channel estimate and estimation error updates given by (3) and (4), respectively, become the dynamic equations

$$d\hat{h}(t) = -\rho \hat{h}(t) dt + \theta(t) \sqrt{\frac{\epsilon(t)}{\sigma_z^2}} d\bar{B}(t), \quad (15)$$

$$\frac{d\theta(t)}{dt} = 2\rho(\sigma_h^2 - \theta(t)) - \frac{\epsilon(t)\theta^2(t)}{\sigma_z^2}, \quad (16)$$

where $\bar{B}(t)$ is a complex Brownian motion independent of $B(t)$, and $\epsilon(t)$ is the pilot power at time t . A heuristic derivation of (13), (15) and (16) from the discrete-time equations (2), (3) and (4) is given in Appendix I.

Note that both $h(t) = h_r(t) + j h_j(t)$ and $\hat{h}(t) = \hat{h}_r(t) + j \hat{h}_j(t)$ are complex. The following SDE defining the evolution of the channel estimate $\hat{\mu}(t) = |\hat{h}(t)|^2 = \hat{h}_r^2(t) + \hat{h}_j^2(t)$ can be obtained

³This bandwidth scaling is simply an interpretation of the effect of the power scaling. The diffusion process is still associated with a *flat* Rayleigh fading channel.

from (15) and a straightforward application of Ito's Lemma [25, Ch. 4]:

$$d\hat{\mu}(t) = \left[-2\rho\hat{\mu}(t) + \frac{\epsilon(t)\theta^2(t)}{\sigma_z^2} \right] dt + 2 \left[\theta(t) \sqrt{\frac{\epsilon(t)}{\sigma_z^2}} \hat{h}_r(t) \right] d\bar{B}_r(t) + 2 \left[\theta(t) \sqrt{\frac{\epsilon(t)}{\sigma_z^2}} \hat{h}_j(t) \right] d\bar{B}_j(t), \quad (17)$$

where $\bar{B}_r(t)$ and $\bar{B}_j(t)$ are, respectively, the real and imaginary parts of the complex Brownian Motion $\bar{B}(t)$. We can re-write (17) as

$$d\hat{\mu}(t) = \left[-2\rho\hat{\mu}(t) + \frac{\epsilon(t)\theta^2(t)}{\sigma_z^2} \right] dt + \theta(t) \sqrt{\frac{\epsilon(t)\hat{\mu}(t)}{\sigma_z^2}} d\underline{B}(t), \quad (18)$$

where $d\underline{B}(t)$ is a *real*-valued standard Brownian motion.

Lemma 1: Given $\epsilon(t) \in [0, \epsilon_{max}]$, the state process $S(t) = (\hat{\mu}(t), \theta(t))$, which is the solution to the stochastic differential equations (18) and (16), has continuous sample paths.

The proof is given in Appendix II. Note that this Lemma does not require the control input $\epsilon(t)$ to be continuous in time. This observation will be useful in the subsequent discussion.

We now consider the continuous-time limit of the optimization problem (9). If the data power for the i^{th} discrete coherence block is P_i/N , then for large (but finite) N , the objective $R(P_i/N, \hat{\mu}_i, \theta_i)$ becomes close to the continuous objective $R[P(t)/N, \hat{\mu}(t), \theta(t)]$, where $R(\cdot)$ is given by (8) and the index i corresponds to time t . Our problem is then to choose $\epsilon(t)$ and $P(t)$, as a function of the state $(\hat{\mu}(t), \theta(t))$, to maximize the accumulated rate function (over time), averaged over the channel process $h(t)$. Equivalently, we can maximize the scaled objective $N R[P(t)/N, \hat{\mu}(t), \theta(t)]$ (corresponding to the sum rate over N parallel sub-channels). A difficulty is that this objective is unbounded as $N \rightarrow \infty$. To simplify the analysis, we first take $N = 1$, which lower bounds the objective for all $N \geq 1$ (and corresponds to scaling up the power in the diffusion limit). After characterizing the optimal policy we then replace the objective with the preceding scaled objective with fixed N to generate numerical results.⁴

We therefore rewrite the discrete-time optimization (9) as the continuous-time control problem

$$\begin{aligned} & \max_{(P(t), \epsilon(t))} \liminf_{t \rightarrow \infty} \frac{1}{t} E \left[\int_0^t R(P(t), \hat{\mu}(t), \theta(t)) dt \right] \\ \text{subject to: } & \limsup_{t \rightarrow \infty} E \left[\frac{1}{t} \int_0^t \epsilon(t) dt + \frac{1}{t} \int_0^t P(t) dt \right] \leq P_{av}, \\ & \text{and } \epsilon(t) \leq \epsilon_{max}. \end{aligned} \quad (19)$$

⁴In Sec. VIII-A we discuss the rate of growth of the scaled rate objective as $N \rightarrow \infty$.

Analogous to (11), the Bellman equation can be written as (see [32])

$$C = \max_{P, 0 \leq \epsilon \leq \epsilon_{max}} \{R(P, \hat{\mu}, \theta) - \lambda(\epsilon + P) + A_\epsilon[V(\hat{\mu}, \theta)]\} \quad (20)$$

where A_ϵ is the generator of the state process $(\hat{\mu}(t), \theta(t))$ with pilot power $\epsilon(t)$ [25, Ch. 7], and is given by

$$A_\epsilon[V] = \frac{E[dV]}{dt} = a + \epsilon b \quad (21)$$

where

$$a = \frac{\partial V}{\partial \hat{\mu}} (-2\rho\hat{\mu}) + \frac{\partial V}{\partial \theta} (-2\rho\theta + 2\rho\sigma_h^2) \quad (22)$$

$$b = \frac{\theta^2}{\sigma_z^2} \left[\frac{\partial V}{\partial \hat{\mu}} - \frac{\partial V}{\partial \theta} + \hat{\mu} \frac{\partial^2 V}{\partial \hat{\mu}^2} \right] \quad (23)$$

and the dependence on t is omitted for notational convenience. Here we ignore existence issues, and simply assume that there exists a bounded, continuous, and twice differentiable function $V(\cdot, \cdot)$ satisfying (20). Note that $V(\cdot, \cdot)$ is unique only up to a constant [20, Ch. 4], [32].

Theorem 1: Given the pilot power constraint $\epsilon \in [0, \epsilon_{max}]$, the optimal pilot power control policy is given by

$$\epsilon^* = \begin{cases} \epsilon_{max} & \text{if } b - \lambda \geq 0 \\ 0 & \text{otherwise.} \end{cases} \quad (24)$$

In words, optimal pilot power control is achieved by a switching (bang-bang) policy. This follows immediately from substituting the generator A_ϵ , given by (21)-(23), into (20), i.e.,

$$C = J(\hat{\mu}, \theta, \lambda) + \max_\epsilon [a + \epsilon(b - \lambda)] \quad (25)$$

where $J(\hat{\mu}, \theta, \lambda) = \max_P [R(P, \hat{\mu}, \theta) - \lambda P]$. Substituting (24) into (25) gives the final version of the Bellman equation

$$C = J(\hat{\mu}, \theta, \lambda) + a + \epsilon_{max}(b - \lambda)^+ \quad (26)$$

where $(x)^+ = \max\{0, x\}$. An alternative way to arrive at (25) and (26) is to take the diffusion limit of the discrete-time Bellman equation (11). This alternative derivation is given in Appendix III.

It is easily shown that the optimal data power allocation is

$$P_d(\hat{\mu}, \theta, \lambda) = \arg \max_P [R(P, \hat{\mu}, \theta) - \lambda P] \quad (27)$$

$$= \left(\frac{-\lambda\sigma_z^2(2\theta + \hat{\mu}) + \sqrt{\Delta}}{2\lambda\theta(\hat{\mu} + \theta)} \right)^+ \quad (28)$$

where $\Delta = \lambda^2 \hat{\mu}^2 \sigma_z^4 + 4\lambda \hat{\mu}^2 \theta \sigma_z^2 + 4\theta^2 \hat{\mu} \lambda \sigma_z^2$ and λ determines P_{av} in (19). Note that $P_d(\hat{\mu}, \theta, \lambda) > 0$ for $\hat{\mu} > \lambda \sigma_z^2$. This power allocation is the same as that obtained in [7], which considers a fading channel with constant estimation error, as opposed to the time-varying estimation error in our model.

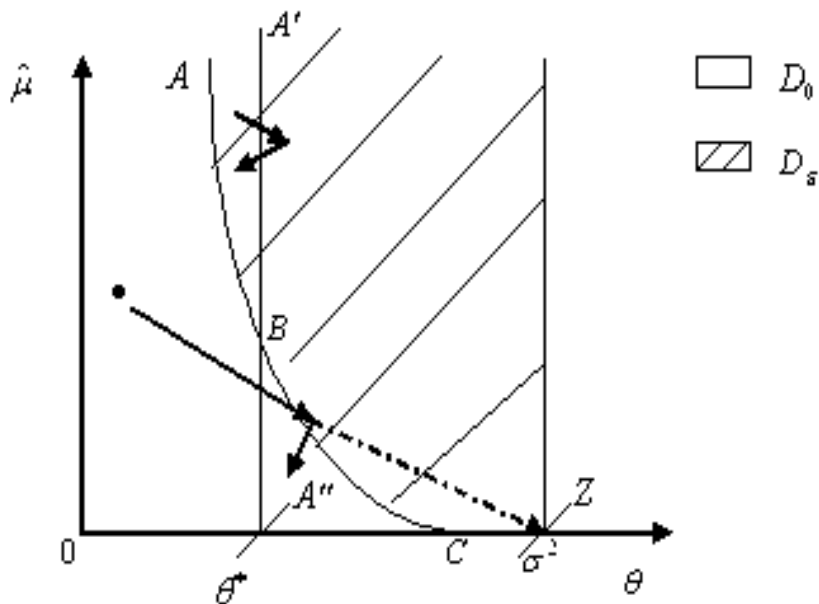


Fig. 1. Illustration of the dynamics of the optimal switching policy for pilot power control.

V. BEHAVIOR OF THE OPTIMAL POLICY

From Theorem 1 the optimal pilot power control policy is determined by the switching boundary in the state space $(\hat{\mu}, \theta)$, which is defined by the condition $b = \lambda$. This is referred to as a “free boundary” condition for the Bellman PDE (20) [27], [28].

The dynamical behavior of the optimal pilot power control policy is illustrated in Fig 1. The vertical and horizontal axes correspond to the state variables $\hat{\mu}$ and θ , respectively. The shaded region, D_ϵ , is the region of the state space in which $\epsilon = \epsilon_{max}$, and $\epsilon = 0$ in the complementary region D_0 . These two regions are separated by the free boundary, AC. The penalty factor λ determines the position of this boundary, and the associated value of P_{av} .

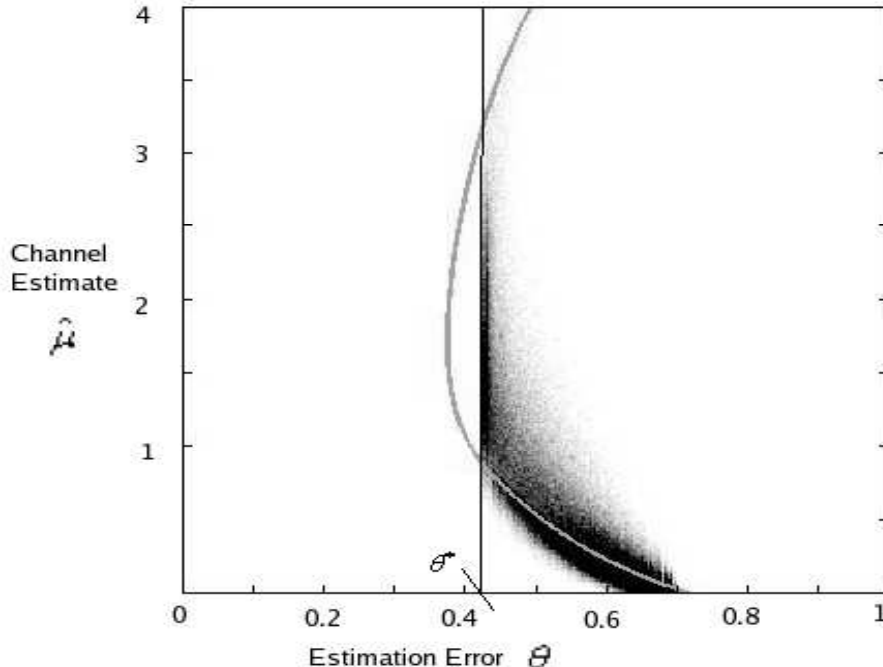


Fig. 2. Trace of the state $(\hat{\mu}, \theta)$ obtained by simulating (18) and (16) with bang-bang control. Parameters are $M = 1, N = 200$, so that $dt = M/N = 0.005$, and $\epsilon_{max} = 12(10.8dB), \rho = 2, \sigma_h^2 = 1, \sigma_z^2 = 1$. A higher density of dots (darker regions) corresponds to higher steady-state probabilities. Also shown is the free boundary computed via the diffusion model. The state lies along the free boundary and the $\theta = \theta^*$ line. Also, the probability decreases with $\hat{\mu}$.

The vertical line $A'A''$ in the figure corresponds to the estimation error variance θ^* , which results from taking $\epsilon = \epsilon_{max}$ for all t . Clearly, in steady state the estimation error variance cannot be lower than this value, hence the steady-state probability density function (pdf) of the state $(\hat{\mu}, \theta)$ is zero for $\theta < \theta^*$. Substituting $\epsilon = \epsilon_{max}$ in (16) and setting $\frac{d\theta}{dt} = 0$ gives

$$\theta^* = (\sqrt{1 + 2\sigma_h^2\gamma} - 1)/\gamma, \text{ where } \gamma = \epsilon_{max}/(\rho\sigma_z^2). \quad (29)$$

Suppose that the initial state is in D_0 . With $\epsilon(t) = 0$ the state evolution equations (18) and (16) become $d\hat{\mu}(t) = -2\rho\hat{\mu}(t)dt$ and $d\theta(t)/dt = 2\rho(\sigma_h^2 - \theta(t))$. This implies that the state trajectory is a straight line towards the point Z until it hits the free boundary, as illustrated in Fig. 1. Therefore, for $P_{av} > 0$, λ must be selected so that the point Z lies in D_ϵ . Otherwise, the state trajectory eventually drifts to Z and stays there, corresponding to $\epsilon = 0$ for all t , $P_{av} = 0$ (because $\hat{\mu} = 0$), and $R = 0$. If the trajectory hits the free boundary below the point B , then it is pushed back into D_0 . This is because at the boundary $\epsilon(t) = \epsilon_{max}$ and for $\theta(t) > \theta^*$, the

drift term in (16) is negative, namely, $d\theta/dt = 2\rho(\sigma_h^2 - \theta(t)) - \frac{\epsilon_{max}\theta^2(t)}{\sigma_z^2} < 0$. Otherwise, if the trajectory hits the boundary above point B , it continues into D_ϵ and settles along the line $A'A''$ where the drift $d\theta/dt = 0$. For the discrete-time model with small, but positive δt , the state trajectory zig-zags around the boundary, as shown in Fig. 1. Hence if the free boundary AC intersects $A'A''$ at point B , then in steady state the probability mass must be concentrated along the curve $A'BC$. This is verified through Monte Carlo simulations and illustrated in Fig. 2. Points in the state space are shown corresponding to a realization generated from (18) and (16) with $M = 1, N = 200$ (so that $\delta t = M/N = 0.005$).

The preceding discussion suggests that the steady-state probability associated with states not on the curve defined by the free boundary and $\theta = \theta^*$ tends to zero in the continuous-time limit. This is stated formally in the next section. We also remark that in region D_0 the PDE (26) is a “transport equation” [27], which has an analytical solution containing an arbitrary function of a single variable. Determining this function and the constant C appears to be difficult, so that we will take an alternative (more direct) approach to determining the free boundary.

VI. STEADY STATE BEHAVIOR WITH SWITCHING POLICY

In this section we characterize the steady-state behavior of the state trajectory with the optimal switching (bang-bang) training policy, and compare with some simpler policies. In particular, we give the first-order pdf over the free boundary, which we subsequently use to compute the optimized boundary explicitly.

We will denote the free boundary as $\theta_\epsilon(\hat{\mu})$ for $\hat{\mu} \geq 0$. To simplify the analysis we make the following assumptions:

(P1) The free boundary $\theta_\epsilon(\cdot) : [0, \infty) \rightarrow (\theta^*, \sigma_h^2)$ is a continuously differentiable curve such that

$$\sigma_h^2 - \theta_\epsilon(x) + \hat{\mu} \frac{d\theta_\epsilon(x)}{dx} \geq 0 \quad \text{for } x \geq 0. \quad (30)$$

(P2) The function $\theta_\epsilon(\cdot)$ is one-to-one, i.e., for any $x_1, x_2 \geq 0$ such that $x_1 \neq x_2$, $\theta_\epsilon(x_1) \neq \theta_\epsilon(x_2)$.

Note that (P1) requires ϵ_{max} to be large enough so that the entire free boundary (AC in Fig. 1) lies to the right of $\theta = \theta^*$. (That is, they do not intersect.) The condition (30) on the derivative of the free boundary curve is mild. Geometrically, it implies that the region enclosed by the

free boundary AC and point $Z = (0, \sigma_h^2)$ is convex. This condition is indeed satisfied by the optimized free boundaries computed in later sections.

Proposition 1: Let the pilot power as a function of the state $(\hat{\mu}(t), \theta(t))$ be given by

$$\epsilon(t) = \begin{cases} \epsilon_{max} & \text{if } \theta(t) \geq \theta_\epsilon(\hat{\mu}(t)) \\ 0 & \text{otherwise.} \end{cases} \quad (31)$$

Then for any $\eta > 0$, the solution to (18) and (16) satisfies

$$\lim_{t \rightarrow \infty} \Pr\{|\theta(t) - \theta_\epsilon(\hat{\mu}(t))| > \eta\} = 0. \quad (32)$$

The proof is given in Appendix IV. The theorem implies that for large t the state $(\hat{\mu}(t), \theta(t))$ moves along the free boundary $\{\theta_\epsilon(\hat{\mu})\}$. Hence for the discrete-time system with large N , the state is typically confined to a narrow strip around the free boundary.⁵

Theorem 2: Given the pilot power control (31), the steady-state probability of training conditioned on the channel estimate $\hat{\mu} = u$ is

$$p(u) = \lim_{t \rightarrow \infty} \Pr\{\theta(t) \geq \theta_\epsilon(\hat{\mu}) | \hat{\mu}(t) = u\} = \frac{2\rho\sigma_z^2[\sigma_h^2 - \theta_\epsilon(u)]}{[\theta_\epsilon(u)]^2\epsilon_{max}}, \quad (33)$$

and the steady-state pdf of the channel estimate $\hat{\mu}$ is

$$f_{\hat{\mu}}(u) = \frac{1}{\sigma_h^2 - \theta_\epsilon(u)} \exp\left(-\int_0^u \frac{1}{\sigma_h^2 - \theta_\epsilon(s)} ds\right), \quad u \geq 0. \quad (34)$$

The proof is given in Appendix V. From (33) the average training power for the pilot power control scheme can be computed as

$$\epsilon_{avg} = \int_0^\infty \frac{2\rho\sigma_z^2(\sigma_h^2 - \theta_\epsilon(u))}{[\theta_\epsilon(u)]^2} f_{\hat{\mu}}(u) du. \quad (35)$$

Therefore if ϵ_{max} is large enough so that $\theta^* < \theta_\epsilon(u)$ for all $u \geq 0$, then neither the pdf $f_{\hat{\mu}}(\cdot)$ nor the average training power ϵ_{avg} depends on ϵ_{max} . This is because as ϵ_{max} increases, the probability of training, given by (33), decreases so that the average training power given $\hat{\mu}$, namely $\epsilon_{max}p(\hat{\mu})$, remains unchanged⁶. In addition, we observe that $f_{\hat{\mu}}(\cdot)$ is independent of the correlation parameter ρ .

⁵This behavior of a controlled Markov process in which the initial state space reduces to a much smaller set under a certain class of control inputs is called "state space collapse" [33].

⁶This ignores the overhead due to the insertion of training symbols. According to the subsequent discussion in Sec. IX, this overhead is reduced by increasing ϵ_{max} . However, for the diffusion approximation to be accurate, $\epsilon_{max} \frac{M}{N}$ must be small, hence ϵ_{max} cannot be too large.

Now consider the case in which the free boundary is constrained to be vertical, that is, $\theta(\hat{\mu}) = \theta_v$, $\forall \hat{\mu} \geq 0$. This still corresponds to a switching policy, but where the variance of the channel estimation error is constrained to be a constant, independent of the channel estimate. From (34) the steady-state pdf of $\hat{\mu}$ is exponential, i.e., $f_{\hat{\mu}}(u) = \frac{1}{\sigma_h^2 - \theta_v} \exp(-\frac{u}{\sigma_h^2 - \theta_v})$, and the average training power is $\epsilon_v = \frac{2\rho\sigma_z^2(\sigma_h^2 - \theta_v)}{\theta_v^2}$.

Now consider the *constant* pilot power control policy, where $\epsilon(t) = \epsilon_v$ (constant) for all t . Substituting $\epsilon = \epsilon_v$ into (16) and setting $\frac{d\theta}{dt} = 0$ implies that the steady-state estimation error variance $\theta(t) = \theta_v$ for all t . In addition, the steady-state pdf of $\hat{\mu}$ is exponential with mean $\sigma_h^2 - \theta_v$. Hence for a given average training power, constant pilot power can give *exactly* the same estimation error and steady-state pdf as the switching policy with a vertical boundary. Both schemes therefore achieve the same rate with a total power constraint (ignoring overhead due to pilot insertion). We will see that the optimized boundary is *not* vertical, which implies that adaptive pilot power control can perform better than constant pilot power.

We also observe that the same performance as the optimal switching policy can be achieved by *continuously* varying the training power as a function of $\hat{\mu}$. Namely, taking $\epsilon(\hat{\mu}) = \frac{2\rho\sigma_z^2(\sigma_h^2 - \theta(\hat{\mu}))}{\theta(\hat{\mu})^2}$ gives the same steady-state pdf and training power as in (34) and (35), respectively. However, this scheme corresponds to feeding back the pilot power as a sequence of real numbers, which in principle require infinite precision. In contrast, the switching policy can be implemented by fixing the training power and varying the rate at which pilot symbols are inserted. The transmitter therefore does not need to know the exact value of the channel estimate.

More specifically, the optimal switching policy inserts pilots of power ϵ_{max} with probability $q = \frac{2\rho\sigma_z^2(\sigma_h^2 - \theta(u))}{\epsilon_{max}\theta(u)^2}$ (or equivalently, once every $1/q$ coherence blocks) when the channel estimate $\hat{\mu} = u$. This requires at most one bit per coherence block to inform the transmitter whether or not to train in the next block. (Of course, the feedback can be substantially reduced by exploiting channel correlations.) The switching policy therefore requires fewer training symbols than continuous pilot power control, which requires a pilot symbol every coherence block.

VII. FREE BOUNDARY WITH OPTIMAL DATA POWER ALLOCATION

From the preceding discussion the optimal pilot policy is determined by the free boundary. Here we compute the free boundary by observing that this boundary must maximize the rate objective, assuming a switching policy for the pilot power. A difficulty is that the rate objective

of interest is $NR(P/N, \hat{\mu}, \theta)$, whereas the steady-state probabilities in Theorem 2 were derived in the limit as $N \rightarrow \infty$. In what follows we use the asymptotic probabilities in Theorem 2 to approximate the steady-state probabilities corresponding to large but finite N . Simulation results have shown that the resulting free boundary is insensitive to the choice of N in the objective. Also, subsequent simulation results in Section VII-C show that the analytical performance results accurately predict the performance of the corresponding discrete-time model with the optimal switching policy when N is a few hundred.

A. Analytical Solution

With the preceding approximation for large but finite N the optimal free boundary can be computed as the solution to the following functional optimization problem,

$$\begin{aligned} & \max_{P(u), \theta_\epsilon(u)} \int_0^\infty NR[P(u)/N, u, \theta_\epsilon(u)] f_{\hat{\mu}}(u) du \\ \text{subject to: } & \int_0^\infty P(u) f_{\hat{\mu}}(u) du + \int_0^\infty \epsilon(u) f_{\hat{\mu}}(u) du \leq P_{av}, \\ & \text{and} \quad \theta_\epsilon(u) \geq \theta^* \quad \text{for } u \geq 0, \end{aligned} \quad (36)$$

where $\epsilon(u) = \frac{2\rho\sigma_z^2[\sigma_h^2 - \theta_\epsilon(u)]}{[\theta_\epsilon(u)]^2}$ can be interpreted as the average training power when the estimate $\hat{\mu} = u$. The objective is the achievable rate averaged over the free boundary since for large N , the entire probability mass becomes concentrated *on* the boundary.

To proceed, define the Lagrangian function as

$$L_\lambda[P, u, \theta] = NR(P/N, u, \theta) - \lambda \left(P + \frac{2\rho\sigma_z^2(\sigma_h^2 - \theta)}{\theta^2} \right) \quad (37)$$

Analogous to (10), the optimization problem (36) can be re-stated as

$$\max_{P(u), \theta_\epsilon(u)} \int_0^\infty L_\lambda[P(u), u, \theta_\epsilon(u)] f_{\hat{\mu}}(u) du \quad (38)$$

such that $\theta_\epsilon(u) \geq \theta^*$ and λ is chosen to satisfy the power constraint (36) with equality. It is shown in Appendix VI that the solution is given by

$$\theta_\epsilon^*(u) = \max\{\theta^*, \theta_f(u)\}, \quad (39)$$

where θ^* is defined in (29), and $\theta_f(u)$ satisfies

$$\begin{aligned} & (\sigma_h^2 - \theta_f(u)) \frac{\partial L_\lambda}{\partial \theta} [NP_d(u, \theta_f(u), \lambda), u, \theta_f(u)] + L_\lambda[NP_d(u, \theta_f(u), \lambda), u, \theta_f(u)] = \\ & \int_u^\infty L_\lambda[NP_d(v, \theta_f(v), \lambda), v, \theta_f(v)] \frac{\exp\left(-\int_u^v \frac{1}{\sigma_h^2 - \theta_f(s)} ds\right)}{\sigma_h^2 - \theta_f(v)} dv \quad (40) \end{aligned}$$

for $u \geq 0$, where

$$\frac{\partial L_\lambda}{\partial \theta} [P, u, \theta] = -\frac{N P^2 u}{(P\theta + Pu + N\sigma_z^2)(P\theta + N\sigma_z^2)} + \frac{2\lambda\rho\sigma_z^2(2\sigma_h^2 - \theta)}{\theta^3} \quad (41)$$

and $P_d(\cdot, \cdot, \cdot)$ is given by (28). The optimal data power allocation is given by $P^*(u) = NP_d(u, \theta_\epsilon^*(u), \lambda)$.

The condition (40) gives the value $\theta_f(u)$ as a functional of the free boundary $\theta_f(x)$ for $x > u$. Hence we can compute the boundary numerically via a backward recursion provided that $\theta_f(u)$ is known for large values of u . Moreover, it can be shown that $\theta_f(u)$ is a decreasing function of u and as $u \rightarrow \infty$, it converges to a constant value, that is, $\theta_f(u) \rightarrow \theta_\infty$. Taking the limit $u \rightarrow \infty$ on both sides of (40), this value can be shown to satisfy

$$\frac{2\lambda\rho\sigma_z^2(2\sigma_h^2 - \theta_\infty)}{\theta_\infty^2} = N \frac{\sqrt{1 + \frac{4\theta_\infty}{\lambda\sigma_z^2}} - 1}{\sqrt{1 + \frac{4\theta_\infty}{\lambda\sigma_z^2}} + 1} \quad (42)$$

Hence as long as ϵ_{max} is large enough so that $\theta^* < \theta_\infty$, the free boundary is given by $\theta_f(u)$, independent of ϵ_{max} .

Substituting $u = 0$ into (40), and using the fact that $\theta_\epsilon^*(u) = \theta_f(u)$ for all $u \geq 0$ (since $\theta^* < \theta_\infty$), and $P^*(0) = 0$, we obtain

$$\frac{[\sigma_h^2 - \theta_\epsilon^*(0)]^2}{[\theta_\epsilon^*(0)]^3} = \frac{1}{4\rho\sigma_z^2} \left[\frac{\bar{R}}{\lambda} - P_{av} \right]. \quad (43)$$

where \bar{R} is the optimized objective in (36). Note that this relation depends on N only through the water-filling level λ . Clearly, the left-hand side of (43) is positive, which implies that we should have $\bar{R} \geq \lambda P_{av}$. Also, as $P_{av} \rightarrow 0$ (low SNRs), $\bar{R} \rightarrow 0$ and λ increases. Similarly, the right-hand side decreases to zero as $\rho \rightarrow \infty$ (fast fading), so that in both cases $\theta^*(0) \rightarrow \sigma_h^2$.

B. Numerical Approach to Free Boundary Problem

The preceding approach to computing the optimal free boundary relies on the asymptotic pdf of the state in Theorem 2. Alternatively, it is possible to solve the continuous-time Bellman equation (26) directly. This is potentially useful for other scenarios in which the steady-state distribution is more difficult to obtain. A challenge, however, is that the optimized free boundary is unknown *a priori*, i.e., it is obtained as part of the solution. Hence none of the standard numerical methods for solving PDEs, which rely on specified boundary conditions, can be directly applied.

It is shown in Appendix VII that a numerical solution to the free boundary Bellman equation can be obtained by re-formulating the problem as a quadratic program. That method can be used

to obtain a solution to a general class of free boundary problems and does not require knowledge of the steady-state statistics. However, such a numerical computation has high complexity, and can be sensitive to parameter variations. In particular, the free boundary obtained from that method is often irregular (not smooth) due to discretization and finite-precision effects.

C. Numerical Results

Here we present some numerical examples of free boundaries obtained by solving the optimization problem (36) along with performance results. The analytical (diffusion) results are also compared with results from a Monte Carlo simulation of the discrete-time system. To solve (36) we discretize the $\hat{\mu}$ axis and also truncate it at a value $U_T \gg \sigma_h^2$. For all of the results in this section $\sigma_h^2 = \sigma_z^2 = 1$, and $\epsilon_{max} = 15$ (11.76 dB). The SNR is then $\frac{P_{av}\sigma_h^2}{\sigma_z^2} = P_{av}$.

a) *Free Boundary Examples:* Fig. 3 shows free boundaries corresponding to $N = 1000$ and $\rho = 2$ for different SNRs. The channel correlation with lag 1000 is therefore $e^{-2} = 0.135$, corresponding to relatively fast fading. (We abuse notation in this section by referring to $\hat{\mu}$ as a particular realization of the channel estimate.) Also shown are the optimized vertical boundaries with a switching policy (i.e., $\theta(u) = \theta_v, \forall u \geq 0$ with optimized θ_v). Recall that the performance with the vertical boundary is the same as training with a constant fraction of power, which results in the estimation error θ_v . For each boundary the data power allocation is given by the optimal water-filling power allocation in (28).

The free boundaries are shaped so that the estimation error is larger for small values of $\hat{\mu}$, and smaller for larger values of $\hat{\mu}$. The reason for this is that the pdf of $\hat{\mu}$ is larger when $\hat{\mu}$ is close to zero where the instantaneous rate $R(\cdot)$ is small. (In fact, $R = 0$ for $\hat{\mu} \leq \lambda\sigma_z^2$.) Allowing larger estimation errors for small $\hat{\mu}$ (relative to the vertical boundary) therefore does not significantly reduce the overall ergodic rate, whereas it saves a significant amount of training power. Furthermore, shifting the savings in training power to larger values of $\hat{\mu}$ reduces the estimation error for those values, thereby increasing the rate (since the rate increases with $\hat{\mu}$). It will be shown in Sec VIII-A that with an optimized on-off power allocation, for large enough N the achievable rate for the free boundary control depends on the shape of the free boundary only through the harmonic mean of the function $\sigma_h^2 - \theta_\epsilon(x)$. This can also be used to show that the boundary has the general shape shown in Fig. 3.

Of course, the estimation error cannot be too large for small $\hat{\mu}$, since otherwise $\hat{\mu}$ may decrease

to zero. (Note from (34) that as $\theta_\epsilon(\hat{\mu}) \rightarrow \sigma_h^2$, the density $f_{\hat{\mu}}(u)$ becomes concentrated around $\hat{\mu} = 0$.) Also, Fig. 3 shows that at smaller SNRs $\theta_\epsilon(0)$ is closer to σ_h^2 , so that the free boundary is more skewed. The curvature of the boundary near $\hat{\mu} = 4$ is a numerical artifact due to truncation of the boundary at $U_T = 5$. Namely, this curvature disappears as U_T increases, since as discussed in the last section, $\theta_f(\hat{\mu})$ is a decreasing function of $\hat{\mu}$ and approaches the value θ_∞ as $\hat{\mu}$ becomes large.

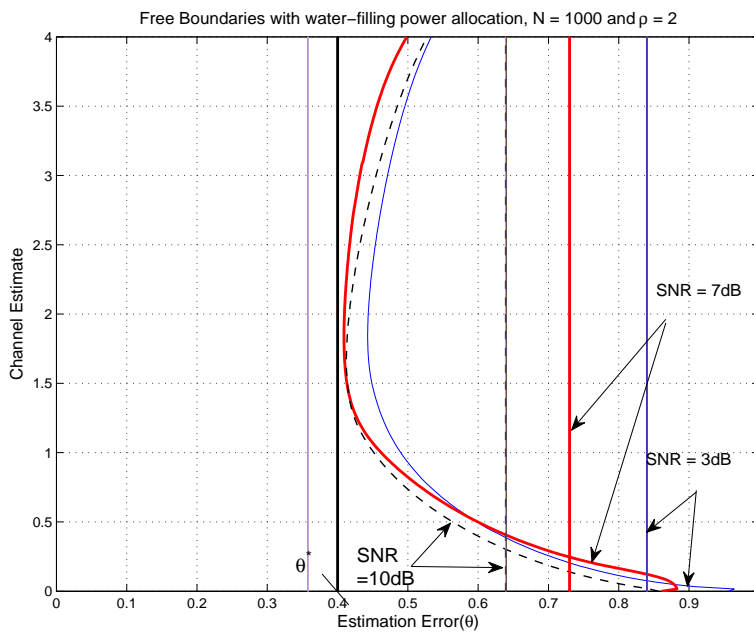


Fig. 3. Optimal free and vertical boundaries with the water-filling data power allocation ($N = 1000$, $\rho = 2$).

b) Gain in Achievable Rate: Fig. 4 compares the rate objective with the optimized free boundary to that achieved with the optimized vertical boundary at different SNRs. With $\rho = 2$ (fast fading) these results show that optimized pilot power control gives substantial gains at low SNRs (e.g., a factor of two at an SNR of 3 dB). The percentage gain diminishes with the SNR. With $\rho = 0.5$, corresponding to a correlation of 0.6 with lag 1000, the gain in achievable rate is relatively small. The optimized free boundary gives the most gain at low SNRs and fast fading, since in that region the training power constitutes a larger percentage of the total power budget.

c) Comparison with Monte Carlo Simulations: Fig. 4 also compares the analytical results from the diffusion model with the performance of the original discrete-time model obtained from

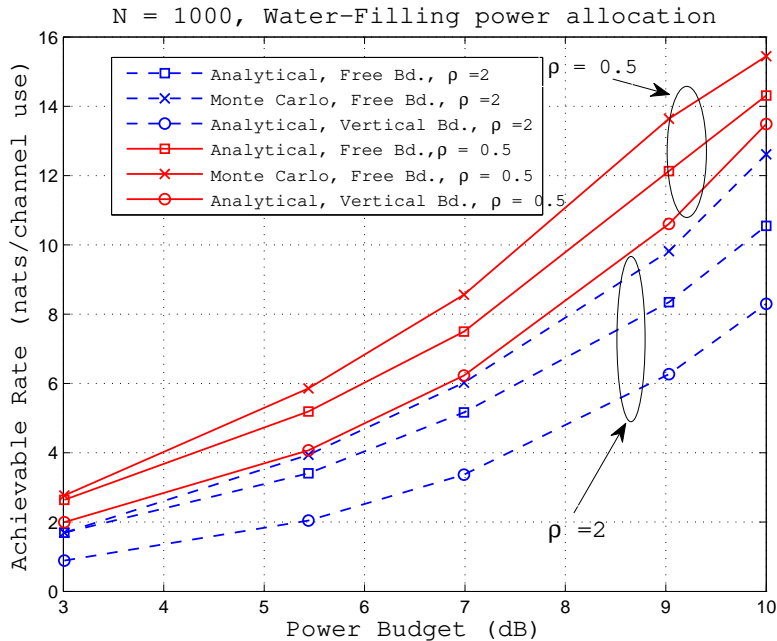


Fig. 4. Achievable rate versus SNR with optimal free and vertical boundary pilot power control.

Monte Carlo simulations. Specifically, the discrete-time system (1)-(2) was simulated with the Kalman filter estimator (3)-(7) and the switching policy for pilot power defined by the optimized free and vertical boundaries.⁷ The comparison in Fig. 4 shows that the analytical results for the optimized free boundary underestimates the achievable rate by about 15-20%. The simulation and numerical optimization give nearly the same values with the optimized vertical boundary.

In addition to the parameters N and ρ , which are the same as for the analytical results, for the discrete-time model another parameter is M , the number of samples per coherence block. Recall that the diffusion model is obtained in the limit as $M/N \rightarrow 0$, hence for fixed N the analytical results should be more accurate for smaller values of M (corresponding to higher correlations between successive channel gains). However, smaller values of M incur more overhead, since the training and channel state feedback occur each coherence block. (We discuss this further in

⁷The simulated results assume the optimized boundaries obtained in the diffusion limit, since the optimized boundary for the discrete-time system, given by the solution to (11), is much more difficult to compute. Additional simulation results have shown that the solution to (11) is quite close to the asymptotic (diffusion) boundary, and gives essentially the same performance.

Sec. IX.) The results in Fig. 4 correspond to $M = 5$.

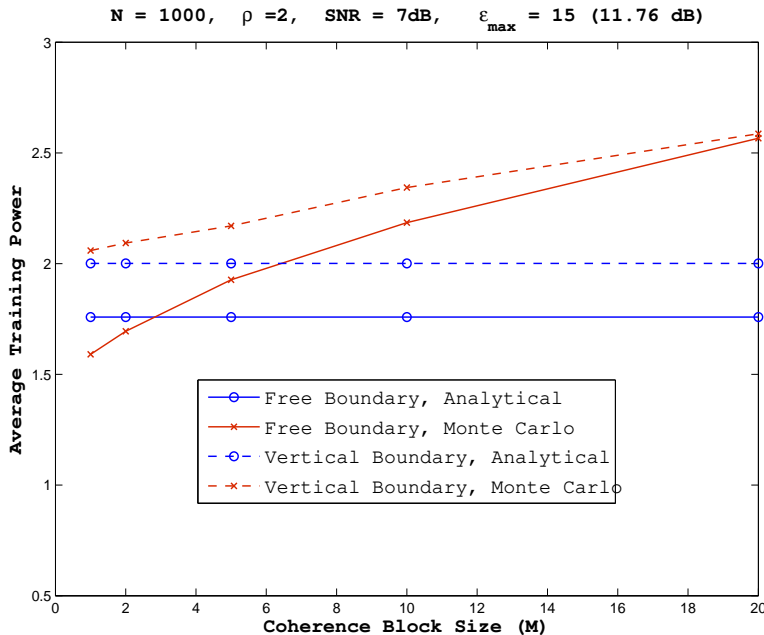


Fig. 5. Comparison of training power values obtained from Monte Carlo simulations and analysis with different values of M . ($N = 1000$, $\rho = 2$ and $SNR = 7dB$)

To see the effect of varying M with fixed N , Fig. 5 compares the optimized average training power obtained via analysis and Monte Carlo simulations for different values of M with an SNR of 7 dB. As expected, the two curves grow apart as M increases, but are reasonably close for $M \leq 5$. Fig 6 compares the simulated steady-state pdf of the channel estimate $\hat{\mu}$ with $M = 5$ with the asymptotic pdf (34). The two curves nearly overlap. Further results show that achievable rates computed from the analytical model nearly match the simulated rates with the vertical boundary over a wide range of M , whereas for the optimized boundary the difference remains similar to that shown in Fig. 4.

Fig. 7 compares analytical and simulated results as a function of N with $M = 1$. For a fixed P_{av} and ρ , as N decreases, the SNR per sub-channel increases and the channel varies at a faster rate since the correlation across N channel uses is fixed at $e^{-\rho}$. The achievable rate increases with N due to the increase in training and channel state feedback. (In Sec. VIII we show that the rate increases as $\log N$.) Again the analytical results closely match the simulated results with

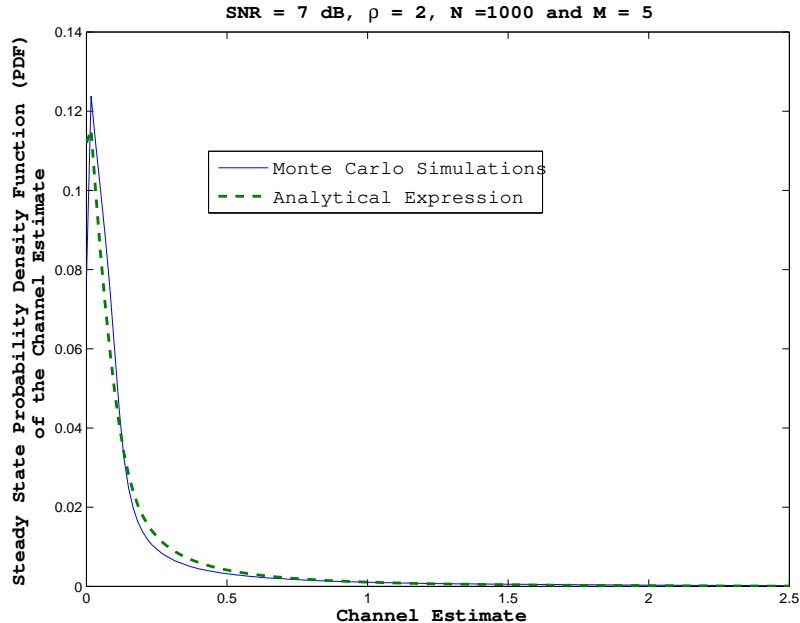


Fig. 6. Channel estimate pdf $f_{\hat{\mu}}(u)$ obtained from Monte Carlo simulations and the diffusion analysis.

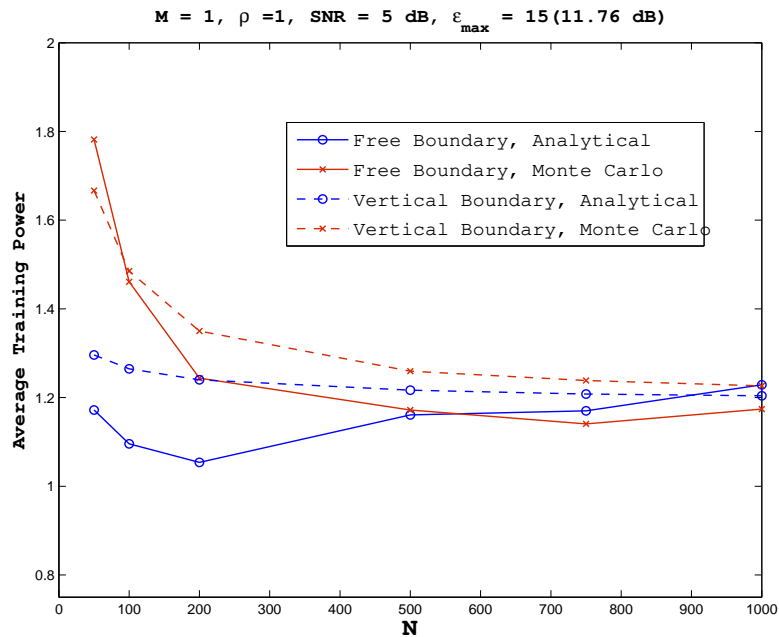
the optimized vertical boundary, and underestimate the achievable rate by 15 – 20% with the optimized free boundary.⁸ The plots for average training power become close for $N \geq 200$.

VIII. ON-OFF DATA POWER ALLOCATION

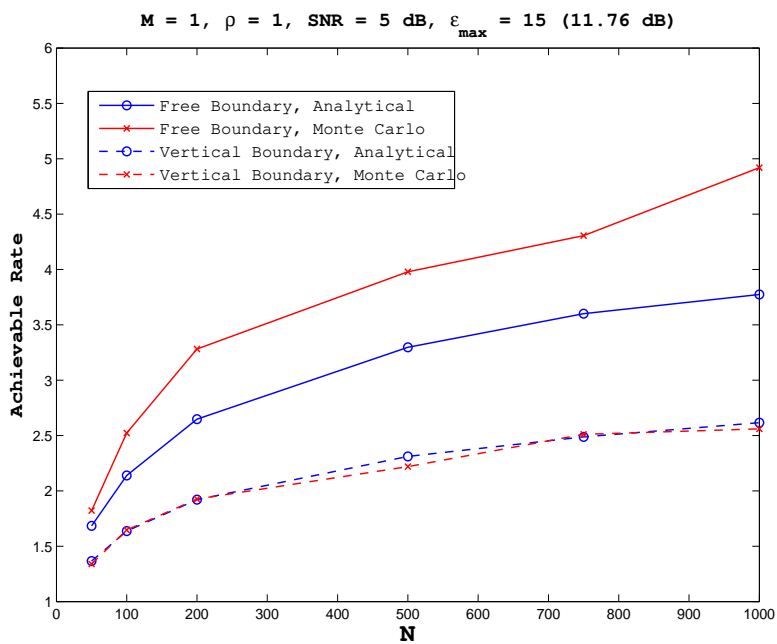
An important consequence of the optimal switching policy for pilot power control is that it requires no more than one bit feedback per coherence block. However, optimal *data* power control still requires infinite-precision feedback. Therefore to reduce the overall feedback rate, we now consider on-off data power allocation, which also requires at most one bit feedback per coherence block. (The feedback could be reduced further by exploiting the time correlation of the channel.) For the optimization problem (36) we therefore set

$$P(u) = \begin{cases} P_0 & \text{if } u > \hat{\mu}_0 \\ 0 & \text{otherwise,} \end{cases} \quad (44)$$

⁸The gap between the analytical and simulation results with the optimized free boundary is due to the fact that as $N \rightarrow \infty$, the scaled rate objective increases without bound. This occurs even though from Theorem 2 the steady-state distribution of the system state converges to the exponential distribution.



(a) Training Power



(b) Achievable Rate

Fig. 7. Comparison of training power and achievable rates obtained from Monte Carlo simulations and the diffusion analysis with different values of N . ($M = 1, \rho = 1, SNR = 5 \text{ dB}$)

where the threshold $\hat{\mu}_0$ will be optimized, and restate (36) as

$$\begin{aligned} & \max_{P_0, \hat{\mu}_0, \theta_\epsilon(u)} \int_{\hat{\mu}_0}^{\infty} NR(P_0/N, u, \theta_\epsilon(u)) f_{\hat{\mu}}(u) du \\ \text{subject to:} & \quad qP_0 + \epsilon_{avg} \leq P_{av}, \\ & \text{and} \quad \theta_\epsilon(u) \geq \theta^*, \quad \text{for } u \geq 0, \end{aligned} \quad (45)$$

where $f_{\hat{\mu}}(u)$ is the steady-state pdf of the channel estimate given by (34), $\epsilon_{avg} = \int_0^\infty \epsilon(u) f_{\hat{\mu}}(u) du$ is the average training power and $q = \Pr\{\hat{\mu} > \hat{\mu}_0\} = \int_{\hat{\mu}_0}^\infty f_{\hat{\mu}}(u) du$.

A. Harmonic Mean Objective

Given a free boundary $\theta_\epsilon(u)$ for $u \geq 0$, where $\theta_\epsilon(u) \in (\theta^*, \sigma_h^2)$, the objective in (45) can be re-written as

$$R_{\text{on-off}}(\hat{\mu}_0) = \int_{\hat{\mu}_0}^{\infty} N \log \left(1 + \frac{(P_{av} - \epsilon_{avg})u}{(P_{av} - \epsilon_{avg})\theta_\epsilon(u) + \sigma_z^2 Nq} \right) f_{\hat{\mu}}(u) du, \quad (46)$$

where we have used the fact that the total power constraint is satisfied with equality. Using (34), the probability of data transmission is

$$q = \int_{\hat{\mu}_0}^{\infty} f_{\hat{\mu}}(u) du = \exp \left(- \int_0^{\hat{\mu}_0} \frac{1}{\sigma_h^2 - \theta_\epsilon(u)} du \right). \quad (47)$$

Furthermore, the rate in (46) can be bounded as

$$Nq \log \left(1 + \frac{(P_{av} - \epsilon_{avg})\hat{\mu}_0}{(P_{av} - \epsilon_{avg})\sigma_h^2 + \sigma_z^2 Nq} \right) \leq R_{\text{on-off}}(\hat{\mu}_0) \leq Nq \log \left(1 + \frac{(P_{av} - \epsilon_{avg})(\hat{\mu}_0 + \sigma_h^2)}{\sigma_z^2 Nq} \right), \quad (48)$$

where the upper bound follows by replacing $\theta_\epsilon(\hat{\mu})$ by 0, using Jensen's Inequality [34], and the fact that $\int_{\hat{\mu}_0}^\infty u f_{\hat{\mu}}(u) du \leq \hat{\mu}_0 + \sigma_h^2$.

Observing that q is a decreasing function of $\hat{\mu}_0$, it can be shown that the upper bound (48) is maximized with threshold $\hat{\mu}_0^*$ such that

$$\int_0^{\hat{\mu}_0^*} \frac{1}{\sigma_h^2 - \theta_\epsilon(u)} du = \log \left(\frac{N}{(\log N)^{1+\delta}} \right) \quad (49)$$

where $\delta \in (0, 1)$ is an increasing function of N . (An exact description of δ is unnecessary for the following analysis.) We can re-write (49) as

$$\hat{\mu}_0^* = H(\hat{\mu}_0^*) \log \left(\frac{N}{(\log N)^{1+\delta}} \right) \quad (50)$$

where $H(\hat{\mu}_0^*) = \frac{\hat{\mu}_0^*}{\int_0^{\hat{\mu}_0^*} \frac{1}{\sigma_h^2 - \theta_\epsilon(u)} du}$ is the *harmonic mean* of $\sigma_h^2 - \theta_\epsilon(u)$ for $u \in [0, \hat{\mu}_0^*]$, that is, along the free boundary truncated at the threshold value $\hat{\mu}_0^*$. Since $H(\hat{\mu}_0^*) \in (0, \sigma_h^2)$, (50) implies that $\hat{\mu}_0^*$ grows as $\log N$. Substituting $\hat{\mu}_0^*$ into (48), we observe that the upper and lower bounds have the same asymptotic growth rate, so that the rate (46) also has this growth rate, given by ⁹

$$R_{\text{on-off}}(\hat{\mu}_0^*) \asymp (\log N)^{1+\delta} \log \left(1 + \frac{(P_{av} - \epsilon_{avg})\hat{\mu}_0^*}{\sigma_z^2 (\log N)^{1+\delta}} \right) \quad (51)$$

$$\asymp \frac{(P_{av} - \epsilon_{avg})\hat{\mu}_0^*}{\sigma_z^2} \quad (52)$$

$$\asymp \frac{(P_{av} - \epsilon_{avg})H(\hat{\mu}_0^*)}{\sigma_z^2} \log N \quad (53)$$

Since $\hat{\mu}_0^*$ maximizes the upper bound in (48), this is the growth rate of the achievable rate.

We observe that this $\log N$ growth in achievable rate is the same as the growth in achievable rate for parallel Rayleigh fading channels (in frequency or time) with a sum power constraint and perfect channel knowledge at the transmitter (e.g., see [35]). This is because the coherence blocks correspond to separate degrees of freedom (i.e., the transmitter can choose whether or not to transmit over each block), and the number of coherence blocks increases linearly with N . For our model the associated constant is $(P_{av} - \epsilon_{avg})H(\hat{\mu}_0^*)$, which accounts for channel estimation error, and depends on the channel correlation ρ . This product therefore determines the shape of the free boundary. (Note also that $\hat{\mu}_0^*$ depends on the free boundary.) Namely, choosing boundary points closer to σ_h^2 reduces ϵ_{avg} , but also reduces the harmonic mean $H(\hat{\mu}_0^*)$, and vice versa. The optimal boundary balances ϵ_{avg} and $H(\hat{\mu}_0^*)$ by shifting training power from small values of $\hat{\mu}$ to larger values, as discussed previously in Sec. VII-C.

B. Numerical Example

Fig. 8 shows free boundaries at different SNRs obtained by solving the optimization problem (45) numerically for $N = 200$ and $\rho = 1$. Also shown are the optimized vertical boundaries with on-off data power control. As with water-filling, the free boundary is shaped to save training power when $\hat{\mu}$ is small (high probability region) and re-distribute it to the instances when $\hat{\mu}$ is large (low probability region). The boundaries shown here are more irregular, due to the discontinuous data power allocation. The shape of the boundary for $\hat{\mu} > \hat{\mu}_0^*$ is a straight line, but does not affect the objective since the rate depends on the harmonic mean for $\hat{\mu} \leq \hat{\mu}_0^*$.

⁹The notation $F_1(N) \asymp F_2(N)$ implies that $\lim_{N \rightarrow \infty} \frac{F_1(N)}{F_2(N)} = 1$.

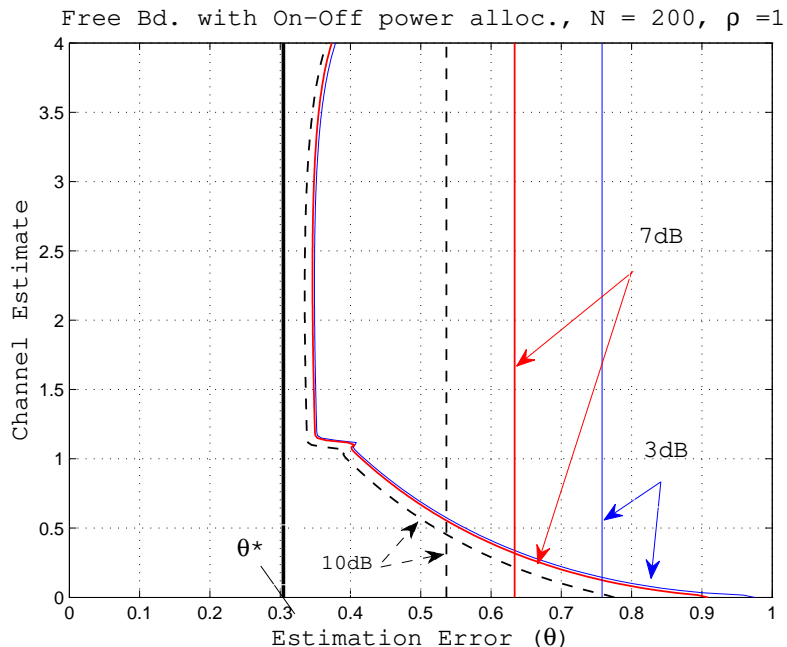


Fig. 8. Optimal free and vertical boundaries with on-off data power allocation.

Fig. 9 shows plots of achievable rates versus SNR with the optimized free and vertical boundaries and on-off data power control. Plots corresponding to the optimal waterfilling data power allocation are also shown for comparison. These results show that the performance with the optimized on-off power allocation are nearly the same as with water-filling. Also shown are the rates obtained via Monte Carlo simulations of the discrete-time system with the optimized boundary. Those are again higher than the rates calculated from the diffusion model, whereas the simulated rates with the vertical boundary closely match the analytical results.

IX. TRAINING SYMBOL OVERHEAD

So far we have ignored the time overhead due to the channel uses that are occupied by the training symbols. Here we restate the pilot power control problem taking this overhead into account. A switching policy for the pilot power requires that one of the M channel uses in a coherence block is a training symbol whenever the transmitter is directed to train. If the channel estimate for the coherence block is $\hat{\mu}$, then the probability of training (as discussed in Sec. VI) is given by $\frac{\epsilon(\hat{\mu})}{\epsilon_{max}}$, where $\epsilon(\hat{\mu}) = \frac{2\rho\sigma_z^2(\sigma_h^2 - \theta_\epsilon(\hat{\mu}))}{\theta_\epsilon(\hat{\mu})}$. Therefore the original optimization problem (36)

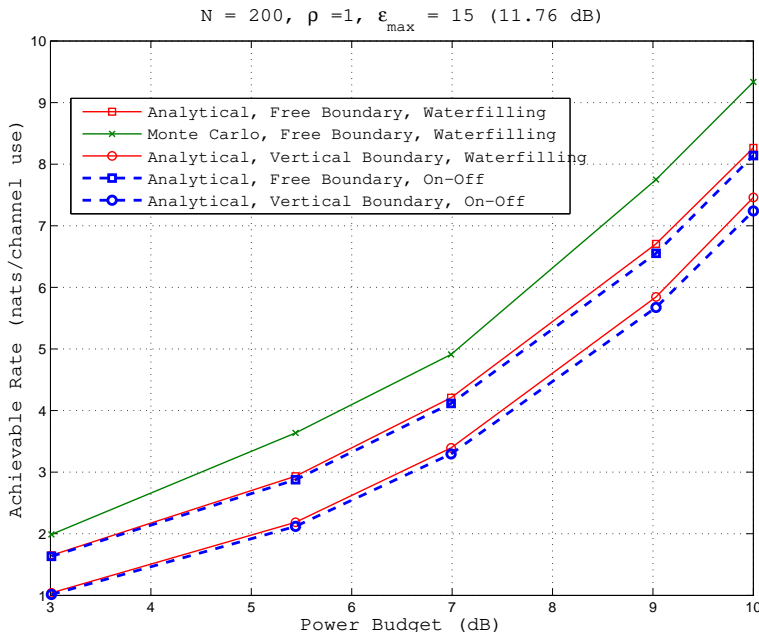


Fig. 9. Achievable rate versus SNR with on-off data power allocation and optimized free and vertical boundaries for pilot power control. Also shown for comparison are the corresponding results with the water-filling data power allocation.

can be reformulated, taking the training overhead in to account, by replacing the rate objective with

$$\max_{(P(u), \theta(u))} \int_0^\infty \left(1 - \frac{\epsilon(u)}{\epsilon_{max} M}\right) NR[P(u)/N, u, \theta(u)] f_{\hat{\mu}}(u) du. \quad (54)$$

Of course, if either ϵ_{max} or M is large, then the training symbol overhead is negligible and the problem reduces to (36). Otherwise, the overhead term will influence the free boundary and ergodic rate. Specifically, it will reduce the optimal training power $\epsilon(\hat{\mu})$ (so that the boundary shifts towards $\theta = \sigma_h^2$), since the overhead penalty is proportional to the training power.

Fig. 10 shows plots of the rate objective in (54) versus SNR with optimized free and vertical boundaries. For this figure $N = 200$ and $M = 1$, corresponding to a worst-case loss in throughput due to training overhead. Also, $\rho = 1$ and $\epsilon_{max} = 15$ (11.76 dB). The data power control is assumed to be on-off and only the analytical results (obtained by maximizing (54)) are shown. (Note that the channel state pdf is still given by Theorem 1.) At low SNRs the average training power and associated overhead are small, so that taking the overhead into account does not significantly affect the rate. At high SNRs (around 10 dB) the training overhead

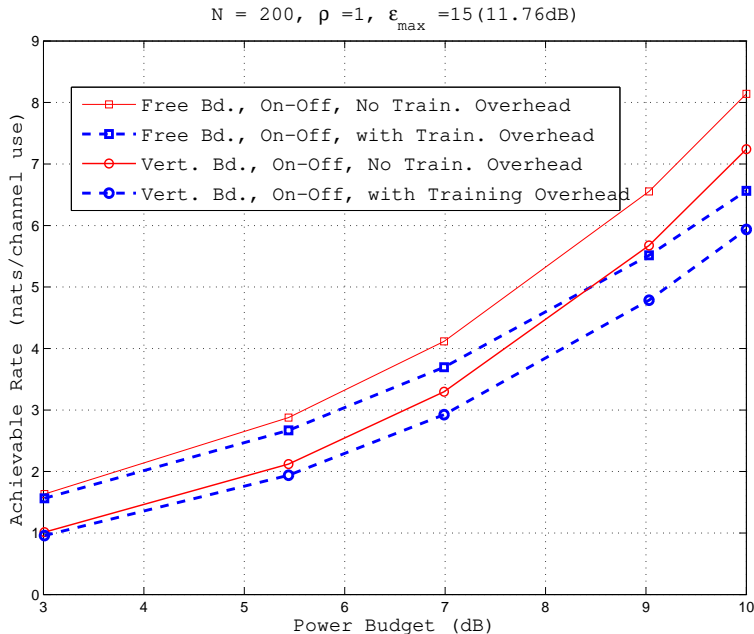


Fig. 10. Achievable rates taking pilot symbol overhead into account.

reduces the achievable rate by about 15% with both the free and vertical boundaries. The percentage improvement provided by the free boundary relative to the vertical boundary remains approximately the same.

A final remark is that when symbol overhead is taken into account, the throughput associated with the vertical switching policy is no longer the same as that associated with constant power control. That is because the switching policy requires on average $\epsilon_{avg}/\epsilon_{max} < 1$ channel uses for training every coherence block, whereas constant power control requires one channel use for training every coherence block. Of course, this savings in overhead for the switching policy comes at the cost of feedback.

X. CONCLUSIONS

We have studied achievable rates for a correlated Rayleigh fading channel, where both the data and pilot power are adapted based on estimated channel gain. In low SNR and fast fading scenarios the pilot power constitutes a substantial fraction of the total power budget, so that pilot power adaptation can provide a substantial gain in achievable rates. By taking a diffusion limit,

corresponding to low SNRs (or wideband channel) and high correlation between consecutive channel realizations, several insights were obtained about the optimal pilot power control policy. Namely, it was shown that a policy that switches between zero and peak training power is optimal, and that the training power should be reduced when the channel is bad and increased when the channel becomes good. The optimal policy in the diffusion limit was also explicitly characterized, and shown to provide a significant increase in achievable rate for low SNRs and fast fading.

For the discrete-time system of interest the switching policy is equivalent to maintaining constant pilot symbol power, but inserting pilot symbols less frequently when the channel estimate is weak (and vice versa). When combined with on-off data power control, this requires finite feedback, and achieves essentially the same performance with the optimal (water-filling) data power control. Of course, the CSI feedback required for optimal data and pilot power control can be substantially reduced by exploiting the correlation between successive coherence blocks.

Several modeling assumptions have been made, which could be relaxed in future work. For example, we have assumed that the receiver knows the statistical model of the channel. In practice, the receiver may assume (or estimate) a model, such as (2), which is mismatched to the actual channel statistics. An issue then is how sensitive this overall performance is to this mismatch. Also, the first-order Rayleigh fading model might be replaced with other fading models (e.g., Ricean, Nakagami, and higher-order autoregressive models).

Additional issues may arise when considering other channel models. For example, here we have imposed a power constraint, which is averaged over many coherence blocks. The results can therefore be directly applied to parallel fading channels where the total power constraint is split among the channels. However, for a frequency-selective channel the total power summed over parallel channels might instead be constrained per coherence block. Other extensions and applications of diffusion models to Multi-Input Multi-Output (MIMO) and multiuser channels remain to be explored.

APPENDIX I

CONTINUOUS-TIME LIMIT OF DISCRETE-TIME PROCESSES (2), (3) AND (4)

Substituting $r = 1 - \rho \delta t$ into (2) and ignoring terms with higher power of δt , we obtain

$$h_{i+1} - h_i = -\rho \delta t h_i + \sqrt{2\rho \delta t} w_i \quad (55)$$

In the diffusion limit the noise $\sqrt{\delta t} w_i$ can be modeled as $dB(t)$, where $B(t)$ is a standard complex Brownian Motion. Hence as $\delta t \rightarrow 0$, the preceding equation becomes (13).

Substituting $r = 1 - \rho \delta t$ in (7) gives

$$\theta_{i+1|i} = (1 - 2\rho \delta t) \theta_i + 2\rho \delta t \sigma_h^2. \quad (56)$$

Replacing ϵ_i by ϵ_i/N in (4) and substituting δt for M/N gives

$$\theta_{i+1} = \left(1 - \frac{\theta_{i+1} \epsilon_i \delta t}{\sigma_z^2}\right) \theta_{i+1|i}. \quad (57)$$

Combining (56) and (57), ignoring the $(\delta t)^2$ term, gives

$$\theta_{i+1} - \theta_i = 2\rho \delta t (\sigma_h^2 - \theta_i) - \frac{\theta_{i+1} \theta_i \epsilon_i \delta t}{\sigma_z^2}, \quad (58)$$

which becomes (16) as $\delta t \rightarrow 0$.

Substituting for r and replacing ϵ_i by ϵ_i/N , (3) can be re-written as,

$$\hat{h}_{i+1} - \hat{h}_i = -\rho \hat{h}_i \delta t + \frac{\theta_{i+1}}{\sigma_z^2} \left[\epsilon_i \delta t (h_{i+1} - \hat{h}_i - \rho \delta t \hat{h}_i) + \sqrt{\epsilon_i \delta t \sigma_z^2} n_{i+1} \right] \quad (59)$$

where, n_{i+1} is a zero mean unit variance CSCG random variable independent of w_i . The term $\frac{\theta_{i+1}}{\sigma_z^2} \epsilon_i \delta t (h_{i+1} - \hat{h}_i)$ is a CSCG random variable with mean zero and variance $\frac{\theta_{i+1}^2}{\sigma_z^4} \epsilon_i^2 E[|h_{i+1} - \hat{h}_i|^2] (\delta t)^2$ and hence can be ignored. Modeling $\sqrt{\delta t} n_{i+1}$ as $d\bar{B}(t)$, where $\bar{B}(t)$ is a standard complex Brownian motion independent of $B(t)$ gives (15) as $\delta t \rightarrow 0$.

APPENDIX II

PROOF OF LEMMA 1

Defining the 3×1 state vector as $\mathbf{G}(t) = [\hat{h}_r(t), \hat{h}_j(t), \theta(t)]^\dagger$, (15) and (16) can be re-written as,

$$d\mathbf{G}(t) = \mathbf{D}[\hat{h}_r(t), \hat{h}_j(t), \theta(t)] dt + \mathbf{V}[\hat{h}_r(t), \hat{h}_j(t), \theta(t)] \bar{\mathbf{B}}(t) \quad (60)$$

where the drift and variance are given by

$$\mathbf{D}(\hat{h}_r, \hat{h}_j, \theta) = \left[-\rho \hat{h}_r, -\rho \hat{h}_j, -2\rho \theta - \frac{\epsilon \theta^2}{\sigma_z^2} + 2\rho \sigma_h^2 \right]^\dagger \quad (61)$$

$$\mathbf{V}(\hat{h}_r, \hat{h}_j, \theta) = \text{diag} \left[\theta \sqrt{\frac{\epsilon}{2\sigma_z^2}}, \theta \sqrt{\frac{\epsilon}{2\sigma_z^2}}, 0 \right] \quad (62)$$

respectively, the dependence on time is dropped for notational convenience, and the three entries of the vector $\bar{\mathbf{B}}(t)$ are independent, real-valued, standard Brownian motions.

From [25, Theorem 5.2.1], given (63) and (64), the solution to (60) exists and is continuous in t provided that the following two conditions are satisfied:

$$|\mathbf{D}(\hat{h}_r, \hat{h}_j, \theta)| + |\mathbf{V}(\hat{h}_r, \hat{h}_j, \theta)| \leq C_1(1 + \sqrt{\hat{h}_r^2 + \hat{h}_j^2 + \theta^2}) \quad (63)$$

$$\begin{aligned} & |\mathbf{D}(\hat{h}_{r1}, \hat{h}_{j1}, \theta_1) - \mathbf{D}(\hat{h}_{r2}, \hat{h}_{j2}, \theta_2)| + |\mathbf{V}(\hat{h}_{r1}, \hat{h}_{j1}, \theta_1) - \mathbf{V}(\hat{h}_{r2}, \hat{h}_{j2}, \theta_2)| \\ & \leq C_2 \sqrt{(\hat{h}_{r1} - \hat{h}_{r2})^2 + (\hat{h}_{j1} - \hat{h}_{j2})^2 + (\theta_1 - \theta_2)^2}, \end{aligned} \quad (64)$$

where for any matrix \mathbf{M} with (k, l) entry \mathbf{M}_{kl} , $|\mathbf{M}| = \sqrt{\sum \mathbf{M}_{kl}^2}$, and C_1, C_2 are constants. Condition (63) is called the linear dominance property and (64) is called the Lipschitz property.

Given $0 \leq \epsilon \leq \epsilon_{max}$, we have

$$|\mathbf{D}| + |\mathbf{V}| = \sqrt{\rho^2 \hat{h}_r^2 + \rho^2 \hat{h}_j^2 + \left(-2\rho\theta - \frac{\epsilon\theta^2}{\sigma_z^2} + 2\rho\sigma_h^2\right)^2} + \sqrt{\frac{\epsilon\theta^2}{\sigma_z^2}} \quad (65)$$

$$\leq \sqrt{\left(2\rho + \frac{\epsilon_{max}\sigma_h^2}{\sigma_z^2}\right)^2 [\hat{h}_r^2 + \hat{h}_j^2 + \theta^2] + 4\rho^2\sigma_h^4 + \frac{\epsilon_{max}\theta^2}{\sigma_z^2}} \quad (66)$$

$$\leq \left(2\rho + \frac{\epsilon_{max}\sigma_h^2}{\sigma_z^2}\right) \sqrt{\hat{h}_r^2 + \hat{h}_j^2 + \theta^2} + \sqrt{4\rho^2\sigma_h^4 + \frac{\epsilon_{max}\theta^2}{\sigma_z^2}}. \quad (67)$$

so that (63) is satisfied. Similarly for $\theta_1 \geq \theta_2$ we have

$$\begin{aligned} & |\mathbf{D}(\hat{h}_{r1}, \hat{h}_{j1}, \theta_1) - \mathbf{D}(\hat{h}_{r2}, \hat{h}_{j2}, \theta_2)| + |\mathbf{V}(\hat{h}_{r1}, \hat{h}_{j1}, \theta_1) - \mathbf{V}(\hat{h}_{r2}, \hat{h}_{j2}, \theta_2)| \\ & \leq \sqrt{\rho^2(\hat{h}_{r1} - \hat{h}_{r2})^2 + \rho^2(\hat{h}_{j1} - \hat{h}_{j2})^2 + \left[2\rho + \frac{2\epsilon_{max}\sigma_h^2}{\sigma_z^2}\right]^2 (\theta_1 - \theta_2)^2 + \frac{\epsilon_{max}}{\sigma_z^2} (\theta_1 - \theta_2)^2}. \end{aligned} \quad (68)$$

so that is (64) satisfied. Since the solution to (18) and (16), $S(t) = (\hat{\mu}(t), \theta(t))$, is a continuous function of $\mathbf{G}(t)$, it must also be continuous in t .

APPENDIX III

ALTERNATIVE DERIVATION OF CONTINUOUS-TIME BELLMAN EQUATION (25)

We first rewrite the discrete-time Bellman equation (11) as

$$C = \max_{(P, \epsilon)} \left\{ R(P, \hat{\mu}, \theta) - \lambda(\epsilon + P) + E_{\epsilon, (\hat{\mu}, \theta)}[V] - V(\hat{\mu}, \theta) \right\}, \quad (69)$$

where

$$E_{\epsilon, (\hat{\mu}, \theta)}[V] - V(\hat{\mu}, \theta) = \int_0^\infty [V(u, \theta_{i+1}) - V(\hat{\mu}, \theta)] f_{\hat{\mu}_{i+1}|S_i}(u) du. \quad (70)$$

Assuming that $V(\hat{\mu}, \theta)$ is a continuous and smooth function, we can expand V around $(\hat{\mu}, \theta)$ via the Taylor series

$$\begin{aligned} V(u, \theta_{i+1}) - V(\hat{\mu}, \theta) &= \frac{\partial V}{\partial \hat{\mu}}(u - \hat{\mu}) + \frac{\partial V}{\partial \theta}(\theta_{i+1} - \theta) \\ &+ \frac{1}{2} \left[\frac{\partial^2 V}{\partial \hat{\mu}^2}(u - \hat{\mu})^2 + 2 \frac{\partial^2 V}{\partial \hat{\mu} \partial \theta}(u - \hat{\mu})(\theta_{i+1} - \theta) + \frac{\partial^2 V}{\partial \theta^2}(\theta_{i+1} - \theta)^2 \right] \\ &+ \text{higher-order terms} \end{aligned} \quad (71)$$

where all the derivatives are computed at $(\hat{\mu}, \theta)$. As stated in Sec. III, $\hat{\mu}_{i+1}$ conditioned on S_i is Ricean, so that

$$f_{\hat{\mu}_{i+1}|S_i}(u) = \frac{1}{\sigma_o^2} e^{-(r^2 \hat{\mu} + u)/\sigma_o^2} I_0 \left(\frac{2\sqrt{r^2 \hat{\mu} u}}{\sigma_o^2} \right), \quad u \geq 0 \quad (72)$$

where $I_0(\cdot)$ is the zeroth-order modified Bessel function of the first kind and

$$\sigma_o^2 = \frac{\epsilon M \theta_{i+1|i}}{\sigma_z^2} \theta_{i+1} \quad (73)$$

where θ_{i+1} and $\theta_{i+1|i}$ are given by (4) and (7), respectively, with θ_i replaced by θ . The first two moments are [36, Ch. 2],

$$E[\hat{\mu}_{i+1} | (\hat{\mu}, \theta)] = r^2 \hat{\mu} + \sigma_o^2 \quad (74)$$

$$E[\hat{\mu}_{i+1}^2 | (\hat{\mu}, \theta)] = 2\sigma_o^4 \left[1 + 2 \left(\frac{r^2 \hat{\mu}}{\sigma_o^2} \right) + \frac{1}{2} \left(\frac{r^2 \hat{\mu}}{\sigma_o^2} \right)^2 \right] \quad (75)$$

Next we take the diffusion limit. Substituting $r = 1 - \rho \delta t$ in (73) and replacing ϵ by ϵ/N gives

$$\sigma_o^2 = \frac{\theta^2 \epsilon}{\sigma_z^2} (\delta t) + O(\delta t^2) \quad (76)$$

Making these substitutions in (74)-(75) gives

$$E[\hat{\mu}_{i+1} - \hat{\mu} | (\hat{\mu}, \theta)] = \left[-2\rho \hat{\mu} + \theta^2 \frac{\epsilon}{\sigma_z^2} \right] \delta t + O(\delta t^2) \quad (77)$$

$$E[(\hat{\mu}_{i+1} - \hat{\mu})^2 | (\hat{\mu}, \theta)] = \left[2\hat{\mu} \theta^2 \frac{\epsilon}{\sigma_z^2} \right] \delta t + O(\delta t^2) \quad (78)$$

It is easily shown that the higher-order moments $E[(\hat{\mu}_{i+1} - \hat{\mu})^n | (\hat{\mu}, \theta)] \leq O(\delta t^2)$ for $n \geq 2$, hence we can ignore the higher-order terms in (71).

Substituting $\theta_i = \theta$ and taking the diffusion limit, (4) can be re-written as

$$\theta_{i+1} - \theta = \left[-2\rho\theta + 2\rho\sigma_h^2 - \theta^2 \frac{\epsilon}{\sigma_z^2} \right] \delta t \quad (79)$$

Substituting (71) into (70) and combining with (77)-(79) gives

$$E_{\epsilon,(\hat{\mu},\theta)}[V] - V(\hat{\mu}, \theta) = \frac{\partial V}{\partial \hat{\mu}} \left[-2\rho\hat{\mu} + \theta^2 \frac{\epsilon}{\sigma_z^2} \right] \delta t + \frac{\partial V}{\partial \theta} \left[-2\rho\theta + 2\rho\sigma_h^2 - \theta^2 \frac{\epsilon}{\sigma_z^2} \right] \delta t + \frac{\partial^2 V}{\partial \hat{\mu}^2} \left[\theta^2 \frac{\epsilon}{\sigma_z^2} \hat{\mu} \right] \delta t \quad (80)$$

Lastly, C , R , ϵ and P can be multiplied by δt without changing the original optimization problem. Applying this scaling in (69), substituting (80) into (69), and multiplying the entire equation by $1/\delta t$ and letting $\delta t \rightarrow 0$ gives (25).

APPENDIX IV

PROOF OF PROPOSITION 1

Define the *distance* from the free boundary at time t as $\kappa(t) = \theta(t) - \theta_\epsilon(\hat{\mu}(t))$. Irrespective of the initial state, due to the drift term in (16) and time continuity of the state process (Lemma 1), with probability one there exists a finite time instant such that the state lies on the free boundary. Without loss of generality, rename that instance as $t = 0$ so that $\kappa(0) = 0$. For any $\eta > 0$ let $t_1 = \inf\{t > 0 : \kappa(t) \leq -\eta\}$. By continuity of the state process, $\kappa(t_1) = -\eta$ and there exists a $t_0 = \sup\{t \in (0, t_1) : \kappa(t_0) = -\eta/2\}$.

If $\kappa(t) < 0$, bang-bang control implies that $\epsilon(t) = 0$ and the dynamical equations (16) and (18) simplify to $d\theta = 2\rho(\sigma_h^2 - \theta)dt$ and $d\hat{\mu} = -2\rho\hat{\mu} dt$. Then

$$d\kappa = 2\rho \left[(\sigma_h^2 - \theta) - \hat{\mu} \frac{d\theta_\epsilon(\hat{\mu})}{d\hat{\mu}} \right] dt, \quad (81)$$

and since $\kappa(t) < 0$ implies $\theta < \theta_\epsilon(\hat{\mu})$, we have $d\kappa > 2\rho \left[(\sigma_h^2 - \theta_\epsilon) - \hat{\mu} \frac{d\theta_\epsilon}{d\hat{\mu}} \right] dt$. Thus given condition (30), we have $d\kappa > 0$ whenever $\kappa(t) < 0$. However, this contradicts the fact that $\int_{t_0}^{t_1} d\kappa = \kappa(t_1) - \kappa(t_0) = -\eta/2$. Therefore we cannot have a $t_1 < \infty$, which implies that $\lim_{t \rightarrow \infty} \Pr\{\theta(t) \leq \theta_\epsilon(\hat{\mu}(t)) - \eta\} = 0$ for any $\eta > 0$.

Next we show that $\lim_{t \rightarrow \infty} \Pr\{\theta(t) \geq \theta_\epsilon(\hat{\mu}(t)) + \eta\} = 0$. For any continuous and twice differentiable function $W(\theta, \hat{\mu})$ we must have [25, Ch. 7]

$$E \{A_\epsilon[W(\theta, \hat{\mu})]\} = 0, \quad (82)$$

where the expectation is over the steady-state distribution of the state $(\theta, \hat{\mu})$. The generator $A_\epsilon[\cdot]$ is defined as in (21), except that the function $V(\cdot)$ is replaced by $W(\cdot)$. We choose $W(\cdot)$ to be

a function of θ only, i.e., $W(\theta, \hat{\mu}) = W(\theta)$, so that

$$A_\epsilon[W] = A_\epsilon[W(\theta)] = W'(\theta) \left[2\rho(\sigma_h^2 - \theta) - \frac{\epsilon\theta^2}{\sigma_z^2} \right] \quad (83)$$

where $W'(\theta)$ denotes the derivative of $W(\theta)$ with respect to θ . Let $p(u)$ denote the steady-state probability of training given that the channel estimate is u , as in (33). Rewriting (82) as

$$E_{\hat{\mu}} E_{\theta|\hat{\mu}} [A_\epsilon[W(\theta)]] = 0, \quad (84)$$

and evaluating the inner conditional expectation using the preceding result that $\Pr\{\theta \leq \theta_\epsilon(\hat{\mu}) - \eta|\hat{\mu}\} = 0$ for any $\eta > 0$ gives

$$\begin{aligned} E_{\hat{\mu}} \{ (1 - p(\hat{\mu})) W'(\theta_\epsilon(\hat{\mu})) [2\rho(\sigma_h^2 - \theta_\epsilon(\hat{\mu}))] \} \\ + E_{\hat{\mu}} \left\{ p(\hat{\mu}) E_{\theta|\hat{\mu}; \theta \geq \theta_\epsilon(\hat{\mu})} \left[W'(\theta) \left(2\rho(\sigma_h^2 - \theta) - \frac{\epsilon_{max}\theta^2}{\sigma_z^2} \right) \right] \right\} = 0 \end{aligned} \quad (85)$$

where $E_{\theta|\hat{\mu}; \theta \geq \theta_\epsilon(\hat{\mu})}[\cdot]$ denotes the expectation over θ given that the estimate is $\hat{\mu}$ and $\theta \geq \theta_\epsilon(\hat{\mu})$. Choosing $W(\theta)$ such that $W'(\theta) = 1 / \left[2\rho(\sigma_h^2 - \theta) - \frac{\epsilon_{max}\theta^2}{\sigma_z^2} \right]$ and substituting in (85) gives

$$E_{\hat{\mu}} \left[(1 - p(\hat{\mu})) \frac{2\rho(\sigma_h^2 - \theta_\epsilon(\hat{\mu}))}{2\rho(\sigma_h^2 - \theta_\epsilon(\hat{\mu})) - \frac{\epsilon_{max}\theta_\epsilon(\hat{\mu})^2}{\sigma_z^2}} \right] + E_{\hat{\mu}} [p(\hat{\mu})] = 0, \quad (86)$$

which implies

$$E_{\hat{\mu}} [(1 - p(\hat{\mu})) 2\rho(\sigma_h^2 - \theta_\epsilon(\hat{\mu}))] = E_{\hat{\mu}} \left[p(\hat{\mu}) \left[\frac{\epsilon_{max}\theta_\epsilon(\hat{\mu})^2}{\sigma_z^2} - 2\rho(\sigma_h^2 - \theta_\epsilon(\hat{\mu})) \right] \right]. \quad (87)$$

Next choose $W(\theta) = \theta$ so that $W'(\theta) = 1$. For this choice (85) gives

$$E_{\hat{\mu}} [(1 - p(\hat{\mu})) [2\rho(\sigma_h^2 - \theta_\epsilon(\hat{\mu}))]] = E_{\hat{\mu}} \left[p(\hat{\mu}) E_{\theta|\hat{\mu}; \theta \geq \theta_\epsilon(\hat{\mu})} \left(\frac{\epsilon_{max}\theta^2}{\sigma_z^2} - 2\rho(\sigma_h^2 - \theta) \right) \right]. \quad (88)$$

We now argue by contradiction that for any $\eta > 0$, $\Pr\{\theta \geq \theta_\epsilon(\hat{\mu}) + \eta|\hat{\mu}\} = 0$ almost everywhere (a.e.) in the set $\mathcal{M} = \{\hat{\mu} : \hat{\mu} > 0\}$. If this were not the case, then we must have $p(\hat{\mu}) > 0$ over a subset in \mathcal{M} with positive measure. Since $\frac{\epsilon_{max}\theta^2}{\sigma_z^2} - 2\rho(\sigma_h^2 - \theta)$ is a positive increasing function of θ , (88) implies

$$E_{\hat{\mu}} [(1 - p(\hat{\mu})) 2\rho(\sigma_h^2 - \theta_\epsilon(\hat{\mu}))] > E_{\hat{\mu}} \left[p(\hat{\mu}) \left(\frac{\epsilon_{max}\theta_\epsilon(\hat{\mu})^2}{\sigma_z^2} - 2\rho(\sigma_h^2 - \theta_\epsilon(\hat{\mu})) \right) \right] \quad (89)$$

with strict inequality, which contradicts (87). Hence this establishes the proposition for any $\eta > 0$.

APPENDIX V
PROOF OF THEOREM 2

As in Appendix IV, we use the fact that for any continuous and twice differentiable function $W(\theta, \hat{\mu})$, we have [25, Ch. 7]

$$E \{A_\epsilon[W(\theta, \hat{\mu})]\} = 0, \quad (90)$$

where the expectation is over the steady-state distribution of $(\theta, \hat{\mu})$ and the generator $A_\epsilon[\cdot]$ is given by (21) with $V(\cdot)$ replaced by $W(\cdot)$. Choosing $W(\hat{\mu}, \theta) = W_1(\theta)$ in (90) to be a function of θ only and applying Proposition 1 gives

$$E_{\hat{\mu}} [W_1'(\theta_\epsilon(\hat{\mu}))g(\hat{\mu})] = 0 \quad (91)$$

where

$$g(\hat{\mu}) = (1 - p(\hat{\mu}))2\rho(\sigma_h^2 - \theta_\epsilon(\hat{\mu})) + p(\hat{\mu}) \left[2\rho(\sigma_h^2 - \theta_\epsilon(\hat{\mu})) - \frac{\epsilon_{max}\theta_\epsilon(\hat{\mu})^2}{\sigma_z^2} \right]. \quad (92)$$

Next we observe that $g(\hat{\mu}) = 0$ a.e. in the set $\mathcal{M} = \{\hat{\mu} : \hat{\mu} \geq 0\}$. If this were not the case, then since $\theta_\epsilon(x)$ is a one-to-one function, we could choose $W_1(\theta)$ such that $W_1'(\theta_\epsilon(\hat{\mu})) = g(\hat{\mu})$, which would make the left-hand side of (91) strictly positive. Therefore setting $g(\hat{\mu}) = 0$ gives the steady-state probability of training given $\hat{\mu}$ shown in (33).

We now solve for the steady-state pdf $f_{\hat{\mu}}(u)$. Choosing $W(\theta, \hat{\mu}) = W_2(\hat{\mu})$, a continuous and twice differentiable function of $\hat{\mu}$ only, and applying the generator (21) gives

$$A_\epsilon[W_2] = -2\rho\hat{\mu}W_2'(\hat{\mu}) + [W_2'(\hat{\mu}) + \hat{\mu}W_2''(\hat{\mu})] \frac{\epsilon\theta^2}{\sigma_z^2}. \quad (93)$$

The necessary condition (90) can now be written as

$$\int_0^\infty [C(u)W_2'(u) + D(u)W_2''(u)] f_{\hat{\mu}}(u) du = 0, \quad (94)$$

where

$$C(u) = -2\rho u + \frac{[\theta_\epsilon(u)]^2 \epsilon_{max}}{\sigma_z^2} p(u) \quad \text{and} \quad D(u) = u \frac{[\theta_\epsilon(u)]^2 \epsilon_{max}}{\sigma_z^2} p(u). \quad (95)$$

We can further choose $W_2(u)$ to satisfy the following properties:

$$W_2(0) = 0 \quad (96)$$

$$\lim_{u \rightarrow \infty} C(u) f_{\hat{\mu}}(u) W_2(u) = 0 \quad (97)$$

$$\lim_{u \rightarrow \infty} D(u) f_{\hat{\mu}}(u) W_2'(u) = 0 \quad (98)$$

$$\lim_{u \rightarrow \infty} \frac{d[D(u) f_{\hat{\mu}}(u)]}{du} W_2(u) = 0 \quad (99)$$

and using integration by parts we can re-write (94) as

$$\int_0^\infty W_2(u) \left(\frac{d^2}{du^2} [D(u) f_{\hat{\mu}}(u)] - \frac{d}{du} [C(u) f_{\hat{\mu}}(u)] \right) du = 0. \quad (100)$$

Since this condition must be satisfied for any such $W_2(\cdot)$, we have

$$\frac{d^2}{du^2} [D(u) f_{\hat{\mu}}(u)] - \frac{d}{du} [C(u) f_{\hat{\mu}}(u)] = 0, \quad \text{a.e. } u \geq 0. \quad (101)$$

Substituting (33) into (101) gives the differential equation

$$\frac{d^2}{du^2} \left\{ 2\rho(\sigma_h^2 - \theta_\epsilon(\hat{\mu})) f_{\hat{\mu}}(u) \right\} - \frac{d}{du} \left\{ [2\rho(\sigma_h^2 - \theta_\epsilon(u)) - 2\rho u] f_{\hat{\mu}}(u) \right\} = 0, \quad \text{a.e. } u \geq 0 \quad (102)$$

which can be further simplified as

$$2\rho[\sigma_h^2 - \theta_\epsilon(u)] u \frac{df_{\hat{\mu}}(u)}{du} + 2\rho u \left(1 - \frac{d\theta_\epsilon(u)}{du} \right) f_{\hat{\mu}}(u) + K = 0, \quad (103)$$

where K is a constant. This is a first-order ordinary differential equation with solution

$$f_{\hat{\mu}}(u) = -K \exp[-I(u)] \int_0^u \frac{\exp[I(t)]}{2\rho[\sigma_h^2 - \theta_\epsilon(t)] t} dt + K_1 \exp[-I(u)], \quad (104)$$

where

$$I(u) = \int_0^u \frac{1 - d\theta_\epsilon(t)/dt}{\sigma_h^2 - \theta_\epsilon(t)} dt \quad (105)$$

$$= \int_0^u \frac{1}{\sigma_h^2 - \theta_\epsilon(t)} dt + \log[\sigma_h^2 - \theta_\epsilon(u)] - \log[\sigma_h^2 - \theta_\epsilon(0)] \quad (106)$$

and K_1 is another constant, which needs to be determined. Since $f_{\hat{\mu}}(u)$ is a pdf, we must have $\lim_{u \rightarrow \infty} f_{\hat{\mu}}(u) = 0$, which implies $K = 0$. This is because the first integral in (104) is unbounded, that is,

$$\int_0^u \frac{\exp[I(t)]}{2\rho(\sigma_h^2 - \theta_\epsilon(t)) t} dt \geq \int_0^1 \frac{1}{2\rho\sigma_h^2 t} dt = \infty. \quad (107)$$

In addition we must have $\int_0^\infty f_{\hat{\mu}}(u) du = 1$, which implies $K_1 = 1/(\sigma_h^2 - \theta_\epsilon(0))$. Substituting these values into (104) gives (34).

APPENDIX VI

DERIVATION OF (39)-(40)

First we fix the free boundary $\theta_\epsilon(\hat{\mu})$ and optimize the data power allocation. For any $\hat{\mu} \geq 0$ setting the derivative of the objective function (38) with respect to $P(\hat{\mu})$ to zero gives the optimal power allocation $P^*(\hat{\mu}) = NP_d(\hat{\mu}, \theta_\epsilon(\hat{\mu}), \lambda)$. Substituting this $P^*(\hat{\mu})$ into (38) and taking the derivative with respect to $\theta_\epsilon(\hat{\mu})$ gives the optimality condition

$$\left[\frac{\partial L_\lambda}{\partial P} [P^*(\hat{\mu}), \hat{\mu}, \theta_\epsilon(\hat{\mu})] \cdot \frac{\partial P^*(\hat{\mu})}{\partial \theta_\epsilon(\hat{\mu})} + \frac{\partial L_\lambda}{\partial \theta} [P^*(\hat{\mu}), \hat{\mu}, \theta_\epsilon(\hat{\mu})] \right] f_{\hat{\mu}}(\hat{\mu}) =$$

$$- L_\lambda [P^*(\hat{\mu}), \hat{\mu}, \theta_\epsilon(\hat{\mu})] \frac{f_{\hat{\mu}}(\hat{\mu})}{\sigma_h^2 - \theta_\epsilon(\hat{\mu})} + \frac{1}{[\sigma_h^2 - \theta_\epsilon(\hat{\mu})]^2} \int_{\hat{\mu}}^{\infty} L_\lambda [P^*(v), v, \theta_\epsilon(v)] f_{\hat{\mu}}(v) dv. \quad (108)$$

Note that $P^*(\hat{\mu}) = 0$ for $\hat{\mu} \leq \lambda\sigma_z^2$ so that $\frac{\partial P^*(\hat{\mu})}{\partial \theta_\epsilon(\hat{\mu})} = 0$. For $\hat{\mu} \geq \lambda\sigma_z^2$ we have $\frac{\partial L_\lambda}{\partial P} [P^*(\hat{\mu}), \hat{\mu}, \theta_\epsilon(\hat{\mu})] = 0$. Therefore (108) reduces to (40) with θ_ϵ replaced by $\theta_f(\hat{\mu})$. The additional constraint $\theta_\epsilon(\hat{\mu}) \geq \theta^*$ implies (39).

APPENDIX VII

FREE BOUNDARY PROBLEM AS A QUADRATIC OPTIMIZATION

We first observe that (26) can be written as the *variational inequality* [28]

$$C - J - a \geq 0$$

$$C - J - a - \epsilon_{max}(b - \lambda) \geq 0$$

$$(C - J - a)(C - J - a - \epsilon_{max}(b - \lambda)) = 0 \quad (109)$$

A solution to (109) is a solution to (26) and vice versa. Now consider the following optimization problem,

$$\min w_0 \int v_1 v_2 d\theta du + \sum_{x \in X} w_x \int [(\partial_x v_1)^2 + (\partial_x v_2)^2] d\theta du$$

$$\text{Subject to : } C - J - a = v_1 \geq 0$$

$$v_1 - \epsilon_{max}(b - \lambda) = v_2 \geq 0 \quad (110)$$

where $\partial_x v_i = \frac{\partial v_i}{\partial x} dx$ for $x \in X = \{\hat{\mu}, \theta\}$ and $i = 1, 2$. If $w_0 > 0$, $w_\theta = 0$, and $w_{\hat{\mu}} = 0$, then the solution to (109) is a solution to (110). Also, a solution to (110) with zero objective value is a solution to (109). The second term in the objective function is included to regularize the

numerical solution. The effect of this term can be controlled by changing the weights w_θ and $w_{\hat{\mu}}$. These weights affect both the accuracy of the results and also the rate at which the non-linear optimization algorithm converges. The training region is where $v_1(\hat{\mu}, \theta) > 0$. Therefore the free boundary can be obtained by solving (110) numerically given values for λ and ρ .

REFERENCES

- [1] D. Tse and P. Viswanath, *Fundamentals of Wireless Communication*. Cambridge University Press, 2005.
- [2] A. J. Goldsmith and P. P. Varaiya, "Capacity of fading channels with channel side information," *IEEE Trans. Inform. Theory*, vol. 43, no. 6, pp. 1986–1992, Nov. 1997.
- [3] G. Caire and S. Shamai, "On the capacity of some channels with channel state information," *Information Theory, IEEE Transactions on*, vol. 45, no. 6, pp. 2007–2019, Sep 1999.
- [4] H. Viswanathan, "Capacity of markov channels with receiver csi and delayed feedback," *Information Theory, IEEE Transactions on*, vol. 45, no. 2, pp. 761–771, Mar 1999.
- [5] J. Liu, N. Elia, and S. Tatikonda, "Capacity-achieving feedback scheme for flat fading channels with channel state information," *American Control Conference, 2004. Proceedings of the 2004*, vol. 4, pp. 3593–3598 vol.4, 30 June-2 July 2004.
- [6] G. Caire, G. Taricco, and E. Biglieri, "Optimum power control over fading channels," *Information Theory, IEEE Transactions on*, vol. 45, no. 5, pp. 1468–1489, Jul 1999.
- [7] T. Klein and R. Gallager, "Power control for the additive white gaussian noise channel under channel estimation errors," *Information Theory, 2001. Proceedings. 2001 IEEE International Symposium on*, pp. 304–, 2001.
- [8] T. Yoo and A. Goldsmith, "Capacity and power allocation for fading mimo channels with channel estimation error," *Information Theory, IEEE Transactions on*, vol. 52, no. 5, pp. 2203–2214, May 2006.
- [9] P. Schramm, "Analysis and optimization of pilot-channel-assisted bpsk for ds-cdma systems," *Communications, IEEE Transactions on*, vol. 46, no. 9, pp. 1122–1124, Sep 1998.
- [10] J. Cavers, "An analysis of pilot symbol assisted modulation for rayleigh fading channels [mobile radio]," *Vehicular Technology, IEEE Transactions on*, vol. 40, no. 4, pp. 686–693, Nov 1991.
- [11] M. Medard, "The effect upon channel capacity in wireless communications of perfect and imperfect knowledge of the channel," *Information Theory, IEEE Transactions on*, vol. 46, no. 3, pp. 933–946, May 2000.
- [12] S. Ohno and G. Giannakis, "Average-rate optimal psam transmissions over time-selective fading channels," *Wireless Communications, IEEE Transactions on*, vol. 1, no. 4, pp. 712–720, Oct 2002.
- [13] B. Hassibi and B. Hochwald, "How much training is needed in multiple-antenna wireless links?" *IEEE Trans. Inform. Theory*, vol. 49, no. 4, pp. 951–963, April 2003.
- [14] A. Bdeir, I. Abou-Faycal, and M. Medard, "Power allocation schemes for pilot symbol assisted modulation over rayleigh fading channels with no feedback," in *Conference Record of the International Conference on Communications (ICC)*, vol. 2, 20-24 June 2004, pp. 737–741 Vol.2.
- [15] M. Dong, L. Tong, and B. Sadler, "Optimal insertion of pilot symbols for transmissions over time-varying flat fading channels," *IEEE Transactions on Signal Processing*, vol. 52, no. 5, pp. 1403–1418, May 2004.
- [16] H. S. Wang and N. Moayeri, "Finite-state markov channel-a useful model for radio communication channels," *Vehicular Technology, IEEE Transactions on*, vol. 44, no. 1, pp. 163–171, Feb 1995.

- [17] H. S. Wang and P.-C. Chang, "On verifying the first-order markovian assumption for a rayleigh fading channel model," *Vehicular Technology, IEEE Transactions on*, vol. 45, no. 2, pp. 353–357, May 1996.
- [18] C. Tan and N. Beaulieu, "On first-order markov modeling for the rayleigh fading channel," *Communications, IEEE Transactions on*, vol. 48, no. 12, pp. 2032–2040, Dec 2000.
- [19] Q. Zhang and S. Kassam, "Finite-state markov model for rayleigh fading channels," *Communications, IEEE Transactions on*, vol. 47, no. 11, pp. 1688–1692, Nov 1999.
- [20] D. P. Bertsekas, *Dynamic programming and optimal control*. Athena Scientific, Vol. 1 and 2, 1995.
- [21] R. Negi and J. Cioffi, "Delay-constrained capacity with causal feedback," *IEEE Trans. Inform. Theory.*, vol. 48, no. 9, pp. 2478–2494, Sep 2002.
- [22] M. Zafer and E. Modiano, "Continuous-time optimal control for delay constrained data transmission," in *Allerton Conference on Communication, Control and Computing, Urbana, IL, USA, September 2005.*, 2005.
- [23] C. Charalambous, S. Djouadi, and S. Denic, "Stochastic power control for wireless networks via sdes: probabilistic qos measures," *Information Theory, IEEE Transactions on*, vol. 51, no. 12, pp. 4396–4401, Dec. 2005.
- [24] R. Berry and R. Gallager, "Communication over fading channels with delay constraints," *IEEE Trans. Inform. Theory.*, vol. 48, no. 5, pp. 1135–1149, May 2002.
- [25] B. Oksendal, *Stochastic Differential Equations: An Introduction with Applications*. Springer-Verlag Berlin Heidelberg, Sixth Edition, 2003.
- [26] T. Feng, T. Field, and S. Haykin, "Stochastic differential equation theory applied to wireless channels," *IEEE Transactions on Communications*, vol. 55, no. 8, pp. 1478–1483, Aug. 2007.
- [27] D. Zwillinger, *Handbook of differential equations*. Academic Press, Third Edition, 1998.
- [28] A. Friedman, *Variational principles and free boundary problems*. Wiley-Interscience, John Wiley and Sons, 1982.
- [29] R. G. Brown and P. Hwang, *Introduction to random signals and applied kalman filtering*. John Wiley and Sons, 1997.
- [30] M. Agarwal and M. L. Honig, "Wideband fading channel capacity with training and partial feedback," in *Allerton Conference on Communication, Control and Computing, Urbana, IL, USA, September 2005.*, 2005.
- [31] W. Whitt, *Stochastic-Process Limits*. Springer, 2002.
- [32] E. Dynkin and A. A. Yushkevich, *Controlled Markov Processes*. Springer Verlag, New York, 1979.
- [33] M. Bramson, "State space collapse with application to heavy traffic limits for multiclass queueing networks," *Queueing Systems: Theory and Applications*, vol. 30, no. 2, pp. 89–148, 1998.
- [34] W. Rudin, *Real and Complex Analysis*. McGraw-Hill Series in Higher Mathematics, Third Edition, 1986.
- [35] Y. Sun and M. L. Honig, "Asymptotic capacity of multi-carrier transmission over a fading channel with feedback," *IEEE Trans. Inform. Theory.*, 2008, to appear.
- [36] J. Proakis and M. Salehi, *Digital Communications*, 5th ed. McGraw-Hill, 2008.